Title
Investigating the Spatiotemporal Properties of Visuomotor Adaptation

Author
Van der Gaag, Gabrielle Lauren

Publication Date
2022

Peer reviewed|Thesis/dissertation

Investigating the Spatiotemporal Properties of Visuomotor Adaptation

By

GABRIELLE LAUREN VAN DER GAAG
THESIS

Submitted in partial satisfaction of the requirements for the degree of

MASTER OF SCIENCE

in

Biomedical Engineering

in the

OFFICE OF GRADUATE STUDIES

of the

UNIVERSITY OF CALIFORNIA

DAVIS

Approved:

Wilsaan M. Joiner, Chair

Lee M. Miller

Jonathon Schofield

Committee in Charge

2022

Abstract

Motivation: Motor adaptation involves utilizing sensory feedback information to modify motor output in response to movement disturbances. This process can occur along a variety of different behavioral aspects (e.g., timeframe: short or long-term changes) and can involve a single effector (unimanual, e.g., brushing your teeth) or multiple effectors (bimanual, e.g., hammering a nail). Understanding the mechanisms underlying sensorimotor adaptation is crucial in developing solutions to motor disorders (e.g., Huntington's Disease, pediatric upper limb deformities, assistive robotics). While there is a well-developed scientific literature basis for unimanual motor learning, there is a gap in understanding the interplay of sensory feedback and external factors such as time delay on adaptation. Additionally, little work has centered around bimanual motor adaptation. By investigating these areas, we may contribute to developing therapeutics and procedures to make daily tasks more accessible to people experiencing motor impairments.

Objective: To (1) investigate the spatiotemporal properties of unimanual visuomotor adaptation through examining the effects of different types of visual feedback (either provided throughout the movement or restricted to only the endpoint) on the local and global components of intra-limb generalization and inter-limb transfer; and (2) provide proof of concept for a method toward further investigation of these properties in multi-manual coordination strategies

Methods: Three motor adaptation experiments were conducted using a custom experimental setup that consisted of an LCD monitor mounted horizontally 20 centimeters above a digitized drawing tablet (12 in x 19 in.; Intuos 3, WaCom) and a 3D printed stylus (2.5 cm diameter). Using the stylus, participants made point-to-point reaching movements on the tablet. View of the reaching arm was obstructed by the monitor. All subjects first underwent a baseline reaching block in which they received full visual feedback of a cursor that directly represented the arm position. Subjects in all three experiments were split into two training groups: those receiving full

visual feedback (FF) (Decay n = 10; Generalization n = 23; Transfer n = 20) and those receiving visual feedback at the onset of the trial and upon reaching the end point only (EPF) (Decay n = 11; Generalization n = 32; Transfer n = 20). In the training block, subjects experienced a visuomotor rotation such that the cursor path deviated ±30° from the hand path. In the decay experiment (Chapter 2), subjects were probed in the absence of visual feedback after a given time delay that varied from 3 to 120 seconds. In the generalization experiment (Chapter 3), subjects moved into a generalization block where the retention of adaptation was probed at different spatial locations (from 0° to ±135° in 15° increments). In the transfer experiment (Chapter 4), subjects were probed using the untrained (left) limb to targets at the different spatial locations outlined above. These studies culminated in the preliminary bimanual motor learning paradigm outlined in Chapter 5 in which subjects were instructed to place a rectangular cursor (1 cm length, 0.5 cm width) in an oriented rectangular target (1.5 cm length, 0.75 cm width) located 12 cm from the starting position using a KINARM robotic manipulandum.

Results: The temporal decay of the adaptation was largely unaffected by the form of visual feedback; retention after a delay of two minutes for endpoint (73.55 ± 7.60%) and full visual feedback (73.43 ± 7.76%) were not significantly different, as well as the respective time constants (τ_{EPF}= 25.31, τ_{FF}= 29.96). Adaptation generalization was best represented by a two-Gaussian model while a single Gaussian model best characterized transfer. Modelling results showed that only the local magnitude of intra-limb generalization was temporally modulated, independent of the feedback condition. In contrast, the spatiotemporal patterns of inter-limb transfer remained near constant across time, again for both types of feedback.

Conclusions: Collectively, these results from Chapters 2-4 suggest that learning mechanisms with different temporal properties underlie the generalization and transfer of visuomotor

adaptation. The results of Chapter 5 confirm the preliminary paradigm as a method of future bimanual coordination and control study.

Keywords: *Motor learning, intra-limb generalization, inter-limb transfer, bimanual coordination*

Table of Contents

Chapter 1: Introduction

1.1: Motor Adaptation

Motor adaptation involves utilizing sensory feedback information to modify motor output in response to movement disturbances (Krakauer et al. 2019). For upper limb movements this may fall under one of two categories: unimanual control (i.e., movements requiring the use of one limb only) (Shadmehr et al. 2010) or bimanual control (i.e., the coordination of movements between the two arms) (Swinnen and Wenderoth 2004; Gooijers and Swinnen 2014). Motor adaptation is commonly examined through perturbation studies in which visual feedback manipulations (via visual prism displacements (Norris et al 2001; Choe and Welch 1974; Shadmehr and Mussa-Ivaldi 1994), or visuomotor rotations (Zhou et al. 2017; Kitago et al. 2013; Joiner et al. 2013; Sisti et al. 2011; Taylor et al. 2011; Howard et al. 2010; Paz et al. 2005; Wang and Sainburg 2004; Anguera et al. 2007; Wang et al. 2015), or imposed force-fields (Rezazadeh and Berniker 2019; Diedrichsen 2007; Nozaki et al. 2006; Shadmehr 2004; Malfait and Ostry 2004; Shadmehr and Moussavi 2000) are applied during movement. The disturbance introduces a source of sensory error that requires adjustments to the motor commands to achieve the desired movement goal. This type of motor learning can be characterized by different properties such as the extent of spatial generalization and transfer of adaptation. Spatial generalization usually refers to the application of the motor learning to motions in the same trained context (e.g., same limb (unimanual) or same control mechanism (i.e., jointly controlled) (bimanual)), but in untrained directions (Shadmehr 2004; Zhou et a. 2017; Shadmehr and Moussavi 2000; Rezazadeh and Berniker 2019; Howard et al. 2010). In contrast, spatial transfer usually describes the extent to which motor adaptation is applied to movements made in a different context (e.g., the untrained limb (Wang and Sainburg 2003; Poh et al. 2016; Joiner et al. 2013; Sainburg and Wang 2002) or application of a unimanual skill in a bimanual setting (Nozaki et al. 2006)). Investigating these properties provides an understanding of the neural mechanisms that underlie initial motor

learning. Within unimanual tasks, generalization provides insight into the spatial tuning of the neural basis elements underlying adaptation and transfer probes the strength and extent of interhemispheric communication (Sainburg and Wang 2002; Anguera et al. 2007; Tanaka et al. 2008). In bimanual tasks, both generalization and transfer provide insight into interhemispheric neural communication - emphasizing the importance of the corpus callosum - and cognitive load involved in inter-manual coordination (Gooijers and Swinnen 2014; Howard et al. 2010; Nozaki et al. 2006).

1.2: Unimanual Motor Learning

1.2.1: Generalization of Adaptation

Previous studies have shown that human motor adaptation of unimanual reaching movements to visuomotor rotations of feedback can be generalized to different target orientations and directions (Paz et al 2005; Taylor et al. 2011; Zhou et a. 2017; Shadmehr and Mousavi 2000). In addition, this generalization has been shown to have a narrow spatial window, such that adaptation generalizes well in directions similar to the trained direction but rapidly decreases the further the movement direction deviates (Shadmehr and Mousavi 2000; Paz et al 2005). Furthermore, other studies have shown evidence that the generalization of adaptation to rotations of visual feedback is comprised of local and global components (Hadjiosif and Smith 2013; McDougle et al. 2017; Zhou et al. 2017). The local component

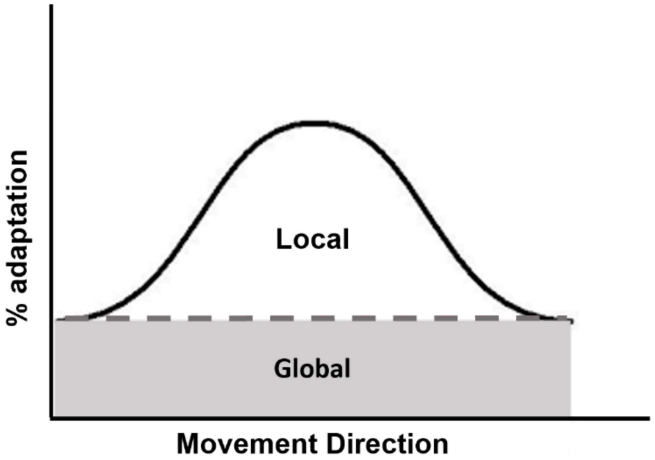

Figure 1: Visualization of local and global components during adaptation generalization. The percent movement adaptation to visuomotor rotation is plotted as a function of movement direction. The center of the x axis represents the trained movement direction – the outer limits of the curve occur at movement directions furthest from the trained direction. The gray shaded area represents the ***global component*** *of adaptation: an adaptation that is applied regardless of movement direction. The region above the dashed line, the* ***local component****, depicts the influence of movement direction on adaptation: greater adaptation localized around the trained direction that dissipates as the reach direction deviates from that training context.*

does not generalize to untrained reaching directions and is specific to the trained movement direction. In contrast, the global component is applied across all movement directions, largely spanning the workspace. Zhou et al. (2017) examined the temporal influence on motor adaptation to a visuomotor rotation and depicted a dual Gaussian model of spatial generalization that suggested interacting global and local components. Additionally, the study demonstrated that the temporal influence on adaptation generalization is largely localized around the trained direction. Paz et al. (2005) suggested that motor adaptation in response to a rotation of visual feedback is largely local while adaptation to a change in visual feedback gain is global. Shadmehr and Moussavi (2000) demonstrated local (movement velocity) and global (arm position) components present in the generalization of adaptation in a force field perturbance.

1.2.2: Transfer of Adaptation

Similar to generalization around target location, many studies have examined the extent of motor adaptation transfer between the limbs (Shadmehr and Mussav-Ivaldi, 1994; Sainburg and Kalakanis, 2000; Sainburg and Wang 2002; Wang and Sainburg 2003; Taylor et al. 2011; Joiner et al. 2013; Wang et al, 2015; Poh et al. 2016). For example, when one limb is trained to adapt to a rotation of movement visual feedback, the transfer of adaptation across the limbs, as quantified by the difference in angular reach trajectory between baseline trials and transfer trials, typically varies between 10 and 60% (Taylor et al. 2011; Wang et al. 2011; Joiner et al. 2013). Transfer is dependent on motor dominance such that the nondominant limb is more effective at end point control but lacks the trajectory refinement of the dominant limb (Sainburg and Kalakanis, 2000; Sainburg and Wang, 2002). In a recent study, Poh et al. (2016) demonstrated that explicit motor learning strategies developed within the trained limb can be fully implemented in the opposite, untrained limb. However, transfer of implicit learning was dependent on the degree to which new sensorimotor maps are spatially compatible for the two limbs. That is, participants'

verbal indication of aiming direction (explicit) more closely aligned with target direction than the observed reach direction (implicit) following transfer. Furthermore, studies have proposed that transferability of the sensorimotor map may provide insight into the neural representations underlying motor learning (Anguera et al. 2007; Tanaka et al. 2008; Sainburg and Wang 2002; Shadmehr 2004; Kitago et al. 2013).

1.2.3: Decay of Adaptation

Adaptation also decays with the passage of time which can be purely passive (time dependent) or active (movement dependent) (Hadjiosif and Smith 2013; McDougle et al 2017; Brayanov et al 2012). In our previous work (Zhou et al. 2017) we demonstrated the influence of time delays on intra-limb spatial generalization of visuomotor adaptation. The results showed that both time and movement modified the spatial application of learning. Interestingly, the global components were shown to be temporally stable where the local components were influenced by time. In an earlier study, Kitago et al. (2013) assessed unlearning under various conditions including the passage of time and introducing error-clamping (trials which visually reflected perfect performance despite any motor error present). Similar to the results in our previous work, they demonstrated that time delay accounts for a small source of unlearning when compared with other performance interference.

The current literature has shown the importance of studying unimanual motor learning in the contexts of spatial generalization (section 1.2.1) and transfer (section 1.2.2); the decay of this learning (section 1.2.3); specificity of motor patterns (i.e., local vs global components); and factors that influence the extent of motor learning (e.g., feedback type). However, these different properties of motor learning are typically studied separately, resulting in a significant gap in understanding the interaction between these various characteristics. Bridging this gap may provide insight into the neural substrates involved in motor learning and could have clinical

applications (e.g., optimizing therapeutic methods for treatment of motor degenerative disorders such as Parkinson's Disease).

1.3: Bimanual Motor Learning

Bimanual control of the limbs is a process involved in the majority of everyday activities which typically involves an unequal distribution of control between the limbs (e.g., hammering a nail) (Swinnen and Wenderoth 2004; Gooijers and Swinnen 2014 for review). Despite the prevalence of inter-manual coordination, existing literature focuses primarily on unimanual motor learning. This emphasis has been proven insufficient in understanding the acquisition of bimanual skills. Nozaki et al. (2006) demonstrated that unimanual learning in a force-field only partially translates to bimanual accomplishment of the same task. After 40 baseline trials in which participants adjusted movement to compensate for an unfamiliar force-field perturbation, randomly dispersed "catch trials" were applied in which the force-field was removed to assess learning retention. Performance was assessed by measuring the "aftereffects" (i.e. the off-center deviation of the reach in the absence of the force-field). Participants demonstrated a 73.8±18.0% decrease in performance within the same limb when trained unimanually and required to transfer the skill to a bimanual task. Alternatively, there was an observed 58.9±11.7% decrease in performance when trained in a bimanual setting and required to transfer the skill to a unimanual task. Similarly, bimanual context (e.g., dual control of a single cursor, individual control of multiple cursors, target location etc.) has proven inextricable from skill development and retention. When trained with a visuomotor rotation in one bimanual context (two, independently controlled cursors moving in the same direction) and required to perform in an opposing context (independently controlled cursors moving in opposite directions), subjects convey an incomplete skill retention similar to that found when transferring from unimanual to bimanual conditions (Howard et al. 2010). Furthermore, the two upper limbs develop an interdependence when tasked with

controlling a single cursor rather than individual cursors. Utilizing force field manipulations, Diedrichsen (2007) found that perturbing one limb in a single cursor condition results in error correction by both limbs whereas the perturbance only affects the disturbed limb in a dual cursor condition. This influence of behavioral context over motor learning likely has further implications on the neural mechanisms of bimanual adaptation (Swinnen 2002; Gooijers and Swinnen 2014).

Though the previously discussed literature provides a foundation, there is a substantial gap in the understanding of how the two hands coordinate control in accomplishing a single task. Importantly, this gap includes relating quantitative behavioral measures to the neural activation patterns that underlie bimanual control and computational models that depict this behavior. Bridging this gap is critical to understanding multi-limb behaviors and will enhance the techniques available to study the neural basis of coordination. Additionally, the anticipated results could have clinical applications (e.g., behavioral biomarkers) and enhance human-robot interactions (e.g., supernumerary robotics).

1.4: Thesis Objectives

This thesis aims to (1) investigate the spatiotemporal properties of visuomotor adaptation through examining the effects of different types of visual feedback (either provided throughout the movement or restricted to only the endpoint) on the local and global components of intra-limb generalization and inter-limb transfer; and (2) provide proof of concept for a method toward further investigation of multi-manual coordination strategies.

This thesis is split into six chapters. **Chapter 1** provides an introduction to motor adaptation and the mechanisms by which it is studied. **Chapter 2** focuses on the time decay of motor learning. **Chapter 3** describes patterns of motor adaptation in a visuomotor rotation paradigm and how this learning generalizes to varied target locations. **Chapter 4** examines the properties of motor behavior when transferred to the untrained limb. **Chapter 5** introduces

preliminary bimanual motor learning data. **Chapter 6** concludes this thesis with a summary of the implications of the work discussed in chapters 2-5 and future goals for this line of research at UC Davis.

Chapter 2: Temporal Decay of Visuomotor Adaptation

2.1: Abstract

Adaptation of motor output in response to visual feedback perturbations decays systematically with the passage of time. This chapter compares the effects of different forms of feedback (provided throughout movement (full feedback) or restricted to only the endpoint (end point feedback)) on the temporal decay pattern of visuomotor adaptation. In the task, subjects moved a screen cursor to a peripheral target and a rotation was applied to the visual feedback of the unseen hand motion. The temporal decay of the adaptation was largely unaffected by the form of visual feedback; retention after a delay of two minutes for endpoint (73.5525 ± 7.598%) and full visual feedback (73.4327 ± 7.7571%) were not significantly different, as well as the respective time constants ($\tau_{EPF} = 25.3138$, $\tau_{FF} = 29.9579$).

2.2: Methods

Participants

Twenty-one healthy participants recruited from the George Mason University population participated in this study. All participants were right-handed and the demographics (e.g., age, gender, etc.) were representative of the University population. Each subject completed only one condition of the experiment. This research was approved by the George Mason University Institutional Review Board. All participants gave informed consent.

Experimental Setup

The details of this protocol are similar to those described in Zhou et al (2017) and Wu and Smith (2013). Participants were seated at a desk facing a custom experimental setup that consisted of an LCD monitor mounted horizontally 20 centimeters above a digitized drawing tablet

(12 in x 19 in.; Intuos 3, WaCom). Chair height was adjusted accordingly so participants could comfortably view the LCD monitor and subjects were positioned so that the center of their body aligned with the center of the setup. Participants grasped a 3D-printed custom cylindrical stylus (2.5 cm in diameter) in their right hand, positioned on the digitized tablet between the tablet surface and an acrylate sheet. The tablet recorded hand position via the stylus at 200 hz.

Experimental Procedure

At the onset of each experiment, each subject received the same baseline and training tasks depicted in Figure 2A. Subjects grasped the cylindrical handle and made point to point movements to peripheral targets on the digitizing tablet. Subjects were tasked with moving the cursor 9 cm from an initial target (5 mm diameter) to an end target (7 mm diameter), both located along the center of the workspace. During the baseline block, the cursor directly represented the position of the hand (Figure 2A). In the subsequent training block, a visuomotor rotation was applied such that the cursor path was rotated about the hand path by either $\theta = +30°$ (CW) or $\theta = -30°$ (CCW) (Figure 2A). Once the radial distance was exceeded, subjects received auditory feedback about the movement speed. The ideal movement duration for this task was predetermined to be between 250 and 400 ms. If subjects reached the target within this timeframe, the target turned green, and the built-in speaker emitted a short-duration beep (429 Hz frequency) to signify a good trial. If the ideal movement duration range was exceeded (≥400 ms), the target turned blue to signify that the movement was too slow. If the cursor reached the target before the ideal minimum (≤250 ms), the target turned red to alert the subject that movement was too fast.

This task, modeled after Hadjiosif and Smith (2012), was designed to assess subjects' retention of angular bias under varying visual feedback conditions. In accordance with the baseline and training protocol common across all experiments (Figure 2D), subjects (n=21) first completed a familiarization block of 20 movements to the trained target located along the

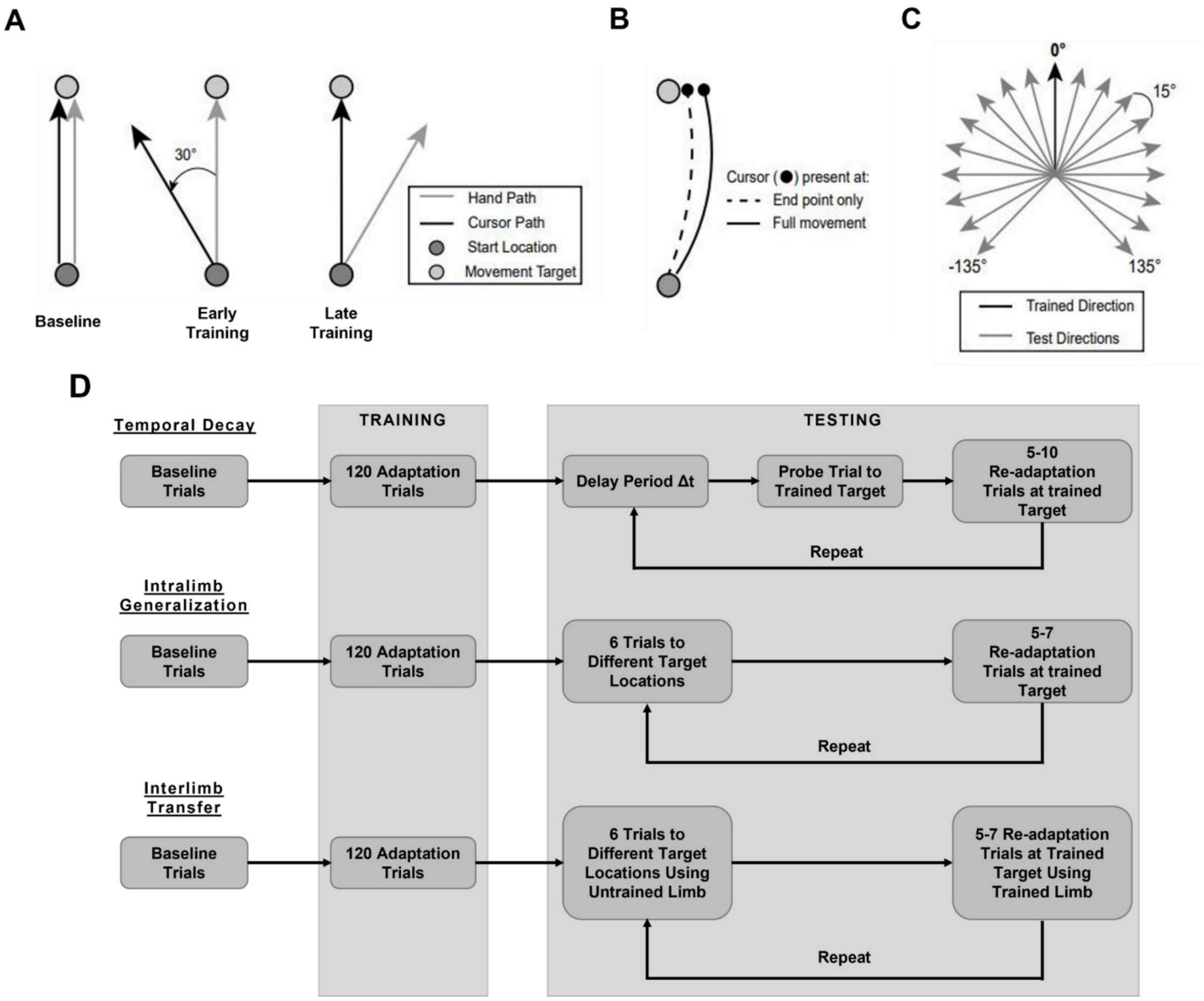

Figure 2: Experimental paradigms and conditions. *A:* Hand vs cursor trajectories before training, in early training and at the end of training. During baseline movements, the cursor directly represents the hand position. A perturbation is applied during training such that there is a 30° rotational offset between the cursor and the hand. *B:* subjects received one of two experimental feedback conditions. In the full feedback condition, participants received constant visual feedback. In the end-point condition, visual feedback is only provided once the movement exceeds the target distance. *C:* movement directions to test the spatial generalization of adaptation. 19 movement directions, separated by 15°, spanning 135° from the trained direction to determine the extent of adaptation transfer. D: experimental protocol outlining the sequence of training and testing blocks for examining the temporal stability, intra-limb spatial generalization, and inter-limb transfer of the trained visuomotor adaptation. Baseline and training blocks are consistent across experiments, but the testing block was unique to each experiment.

horizontal axis of the workspace (0° position in Figure 2C) with full visual feedback. A subsequent baseline block consisted of 24 movements to the trained target wherein 25% of the trials were randomly selected to be blank trials – trials where the cursor targets were displayed on the screen

at movement onset and removed when reach speed exceeded 5 cm/s such that no visual feedback was provided (blank screen) during or at the completion of movement. These six blank trials served as the baseline for the retention probe trials.

Upon completion of the baseline trials, subjects entered the training block of 120 adaptation trials. Subjects were assigned to one of two experimental groups: 11 subjects were assigned to continue to receive full visual feedback during trials and 10 subjects were to receive end point visual feedback only. At the onset of the training block, subjects completed 15 baseline movements to the trained target, receiving feedback in accordance to the designated group. On the 16th movement, a visual perturbation of $\theta = +30°$ or $\theta = -30°$ was abruptly applied at the movement feedback point such that the final position of the cursor was rotated about the final hand position by the designated angular offset.

After the training block, subjects completed retention probe and retention trials. Subjects were assessed following 8 delay periods (0, 3, 6, 10, 20, 30, 60, and 120 seconds). During the delay, subjects held the cursor in the start target until prompted to move by a reach target appearing on the screen. The first of these retention trials was a probe trial characterized by the absence of any visual feedback. This blank trial was followed by 5-10 readaptation trials in which subjects' visual feedback was restored in accordance with the assigned experimental group. This pattern of a delay, single retention probe, and 5-10 retraining trials was repeated 32 times such that each delay period was probed four times. Because of the randomness of the number of retraining trials, subjects completed a total of 250-320 movements divided among the three blocks.

Analysis

For each reaching movement, the hand position was recorded at 1 cm and 3 cm into the reach. The movement angle was calculated as the angular offset of the line connecting these two points from the 0° trajectory. The percent adaptation for the training block was then calculated as the ratio of this movement angle to the magnitude of the visual perturbation ($\theta = \pm 30°$). For probe

trials, subject performance was evaluated based on adaptation retention following the experimental time delay (i.e., comparing two ratios: (1) the ratio of movement angle to the magnitude of the trained perturbation for the probe trial and (2) the percent adaptation during learning). All trials greater than two standard deviations from the mean for each subject were removed from analysis. To determine the changes in retention across the eight delay periods we applied a standard exponential function:

$$r(t) = a \cdot e^{-\frac{t}{\tau}} + b$$

where a is the scaling factor, b is the offset and τ is the time constant. We examined the time constant across experimental conditions (end-point vs full visual feedback) to determine the influence of feedback type on the temporal stability of motor learning. The coefficient of determination (R^2) was used to quantify the goodness of fit.

Data were analyzed offline using Matlab 2019a (The MathWorks, Natick, MA) and R 3.6.2 (r-project.org). Trials that had very slow/fast movement speeds (peak speed < 0.2 m/s or > 0.5 m/s) were excluded. We tested the main effect of group (full feedback and endpoint feedback) on the amount of adaptation with a linear mixed effects model (LMM) in R using the lmerTest package (Kuznetsova et al. 2014) with the fixed effects of group (full feedback and endpoint feedback) and period (different trial periods in the experiment, e.g., early learning, middle learning, and late learning period; first 10, middle 10 and last 10 training trials, respectively) and random effect of subjects. The model was estimated using the restricted maximum likelihood method (REML) and the significance was obtained using Kenward-Roger and Satterhwaite's approximations with pbkrtest package (Halekoh et al. 2014). If significance was identified, post hoc tests were performed using the emmeans package and adjusted for multiple comparisons using Bonferroni-Holm corrections. Effect size (d) was calculated using Cohen's d (Cohen 1988) measurement (for LMM analysis, generalized effect size was computed following similar procedures of Cohen's d measurement using the eff_size function in the emmeans package). For all tests, the significance

level was set to 0.05. In all cases, group data are presented as mean±SEM and estimation of the proposed model coefficients were reported with 95% confidence intervals.

2.3: Results

2.3.1 Learning Curves

Across both feedback conditions, we observed an exponential learning curve (Figure 3) similar to those in previous studies (Zhou et al. 2017; Taylor et al. 2011) with a rapid adaptation increase during early learning and a plateau after ~50 trials. An LMM (see Analysis in section 2.2) was used to investigate the fixed effects of feedback group (full feedback and endpoint feedback) and training period (early and late) and random effect of subjects on the percent adaptation during training. There was not a significant difference in learning between groups receiving endpoint feedback only when compared with those that received full feedback ($t.ratio = -0.31, P_{EPF/FF} > 0.75$). In both conditions, there was a significant increase ($P_{FF}, P_{EPF} < 0.01$) in the adaptation percentage from early training (FF: 19.8 ± 1.3% EPF: 18.4 ± 1.1%) to late training (FF: 92.5 ± 2.3% EPF: 93.2 ± 0.9%). These results suggest that motor adaptation in this visuomotor rotation is independent of feedback type.

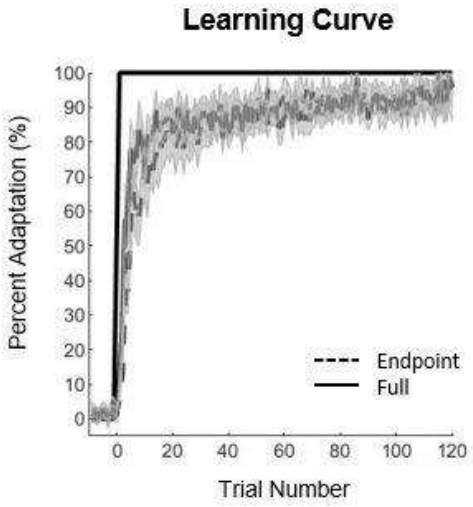

Figure 3: Learning curves during training for the temporal decay experiment. The solid black line represents mean % adaptation of all participants in the full feedback group for each trial number. The dashed black line represents mean % adaptation of all participants in the endpoint feedback group for each trial number. The gray shaded area represents the standard error. The black step function represents the magnitude of the perturbation.

2.3.2 Temporal Decay Curve

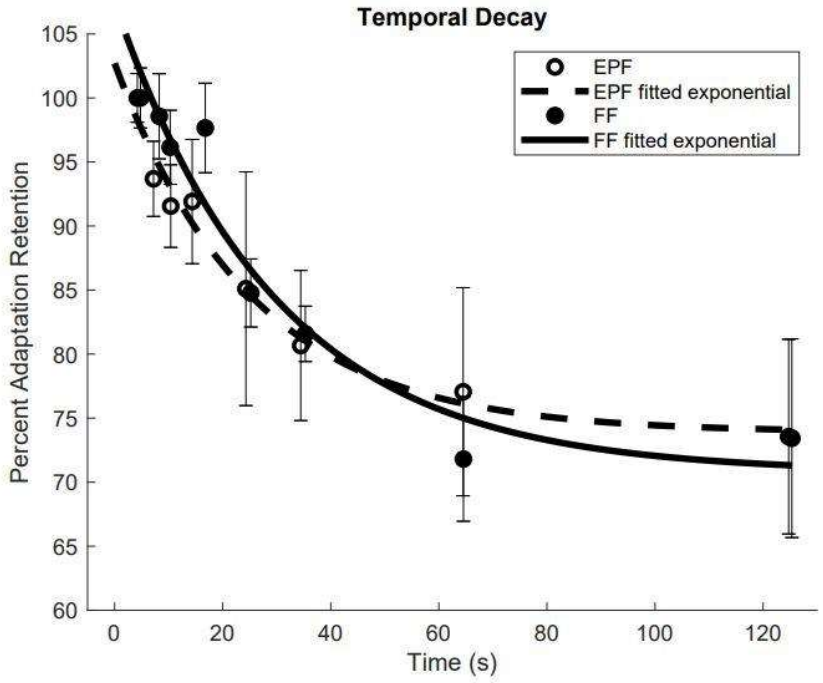

Figure 4: Adaptation decay over time. Percent adaptation retained after each temporal delay is plotted as a function of time. The solid line represents the fitted exponential for the full feedback data. The dashed line represents the fitted exponential for the endpoint feedback data. The filled circles and open circles represent mean full feedback and mean endpoint feedback data respectively across all participants. Both the percent adaptation and delay times are averaged across participants in their respective feedback groups. Error bars represent the standard error.

When looking at the influence of feedback conditions on the extent of adaptation retention after various time delays, we observed that the angular deviation applied to the reaching movement systematically decayed in both endpoint and full feedback conditions (Figure 4). The duration of the delay had a significant effect on the adaptation retention ($F(118,1)=44.25$, $P<0.0001$) such that an exponential decay model reliably fit the data ($r^2_{EPF} = 0.95$ $r^2_{FF} = 0.98$) with a time constant of $\tau_{EPF} = 25.31 \pm 12.34$ for the endpoint condition and $\tau_{FF} = 29.95 \pm 25.31$ in the full feedback group. Reaching movements following the shortest tested time delay ($\Delta t=3s$) followed adaptation conditions that were not significantly different from those at the end of training (FF retention: 100 ± 2.35% EPF retention: 100 ± 1.90%). When tested after the longest time delay ($\Delta t=120s$), subjects demonstrated significant decay in learning (FF retention: 73.43 ± 7.76% EPF retention: 73.55 ± 7.60%). Although subjects receiving full visual feedback had a more rapid decay

in adaptation, there was no significant difference between the two groups (t.ratio=-0.8, P > 0.42). These results suggest that the retention of visuomotor adaptation over time is not significantly impacted by the type of visual feedback provided.

Chapter 3: Spatiotemporal Properties of Intra-limb Generalization of Visuomotor Adaptation

3.1: Abstract

In addition to the systematic temporal decay of motor adaptation, intra-limb spatial generalization of such learning is selectively modified by time; learning applied near the trained movement direction (±15°) decreases with time while generalization further away (>60°) remains near constant. This chapter compares the effects of different forms of feedback (provided throughout movement or restricted to only the endpoint) on these spatiotemporal relationships for intra-limb generalization. In the task, subjects moved a screen cursor to a peripheral target and a rotation was applied to the visual feedback of the unseen hand motion. The generalization of adaptation was assessed at 19 different locations (spaced 15° apart, symmetric around the trained direction) and examined following three delays (approximately 4, 12, and 25 s). Adaptation generalization was best represented by a two-component Gaussian model. Modelling results showed that only the local magnitude of intra-limb generalization was temporally modulated, independent of the feedback condition.

3.2: Methods

Participants

Fifty-five healthy participants recruited from the George Mason University population participated in this study. All participants were right-handed and conducted the task with their right hand only. The demographics (e.g., age, gender, etc.) were representative of the University population. Each subject completed only one condition of the experiment. This research was

approved by the George Mason University Institutional Review Board. All participants gave informed consent.

Experimental Setup and Procedure

The details of the experimental setup are the same as described in section 2.2. Modeled after Brayanov et al. (2012), this task was designed to determine the feedback dependency of the spatial characteristics of the generalization of visuomotor adaptation. As depicted in Figures 2A and 2D, all subjects first entered a baseline block of 19 familiarization movements – one to each reach target position (spanning -135° to +135° in 15° increments). Similar to the baseline for the Temporal Decay Experiment (outlined in section 2.2.3), a subsequent baseline block was completed with randomized blank trials to establish a baseline for following retention probe trials. This block consisted of 4 movements to each target location for a total of 76 movements. Two of the four movements to each target location were randomly selected as blank trials. This baseline block was repeated three times for a total of 228 movements.

Following the baseline, subjects were trained with the visual perturbation. Subjects were randomly selected to be in one of two feedback groups: full visual feedback (n=23) and endpoint visual feedback (n=32). The training period for this task began with an initial 15 movements to the trained target under baseline conditions with participants receiving feedback as designated by their group assignment. On the 16th movement, the ±30° rotational perturbation was applied to the path of cursor motion. Each subject completed a total of 120 movements to the trained target in the 90° location.

After the training period, all subjects continued to generalization probe trials in which they completed movements in the absence of visual feedback (blank trials) to 6 pseudo-randomly selected target locations. In these blank trials, the cursor and target locations were visible until reach speed exceeded 5 cm/s, at which point visual information was removed from the screen; no feedback was provided at the end of the trial. Participants were subsequently retrained in 5-7

trials, receiving their assigned feedback. This process of 6 probe trials followed by 5-7 retraining trials was repeated until each of the 19 movement directions was tested in each of the 6 different placements within the probe sequence. That is, each movement direction was tested for generalization early (probe 1), late (probe 6), and at each time in between (probes 2-5). As such, subjects completed a total of 209-247 movements between the three blocks. These probe trials took place within 25-35 seconds of the final training/retraining trial. From the set of probe trials, we defined three general delay periods with 95% confidence intervals (4.4 ± 1.6, 12.0 ± 4.2, 24.6 ± 8.6 s) to determine the effects of elapsed time on the spatial generalization of motor adaptation.

Analysis

For each reaching movement, the movement angle and percent adaptation were calculated as described in section 2.2. For probe trials, subject performance was evaluated based on how well subjects maintained adaptation (i.e. comparing performance to the following experimental condition). Adaptation generalization was determined by finding the ratio of movement angle to target location angle for reaching movements to untrained locations and comparing this to the percent adaptation of the trained limb at the end of training.

Computational modelling

A modified two Gaussian model was applied to provide a general representation of the changes in the spatial relationships across the different conditions in the intra-limb generalization experiments (Brayanov et al. 2012; Zhou et al. 2017). The two Gaussian model:

$$z(\theta) = k_1 e^{-\frac{|\theta-\theta_0|^2}{2\sigma_1^2}} + k_2 e^{-\frac{|\theta-\theta_0|^2}{2\sigma_2^2}} + c$$

is representative of the amount of generalization (z) to a given target direction (θ) and accounts for the interaction of local and global components during motor learning. Generalization is dependent on the magnitudes of adaptation to two local (k_1, k_2) components at the peak movement direction (θ_0). Similarly, the width of the model is influenced by two local (σ_1, σ_2)

components. The offset term (c) represents the amount of constant generalization to all movement directions due to the global component.

Statistics

Data were analyzed offline using Matlab 2019a (The MathWorks, Natick, MA) and R 3.6.2 (r-project.org). Trials that had very slow/fast movement speeds (peak speed < 0.2 m/s or > 0.5 m/s) were excluded (~10% of total trials for full feedback group and ~7% of total trials for endpoint feedback group). We tested the main effect of group (full feedback and endpoint feedback) on the amount of adaptation with a linear mixed effects model (LMM) in R using the lmerTest package (Kuznetsova et al. 2014) with the fixed effects of group (full feedback and endpoint feedback) and period (different trial periods in the experiment, e.g., early learning and late learning period; first 10% and last 10% of training trials, respectively) and random effect of subjects. The model was estimated using the restricted maximum likelihood method (REML) and the significance was obtained using Kenward-Roger and Satterhwaite's approximations with pbkrtest package (Halekoh et al. 2014). If significance was identified, post hoc tests were performed using the emmeans package and adjusted for multiple comparisons using Bonferroni-Holm corrections. Effect size (d) was calculated using Cohen's d (Cohen 1988) measurement (for LMM analysis, generalized effect size was computed following similar procedures of Cohen's d measurement using the eff_size function in the emmeans package). For all tests, the significance level was set to 0.05. In all cases, group data are presented as mean±SEM and estimation of the proposed model coefficients were reported with 95% confidence intervals.

To quantify the goodness of fit for the spatial generalization of adaptation model described above, we fit the function with different subsets of free parameters and computed the Akaike information criterion (AIC) for each model (Akaike 1974). The generalization data set was fit with the two-Gaussian model and a single Gaussian model (see section 4.2.2). This allowed us to determine the best fit model for the motor learning task as well as which parameters are temporally influenced. First, the peak movement direction (θ_0) was set to the trained movement

direction. In the case of the two-Gaussian model, the five parameters (k_1, k_2, σ_1, σ_2, and c) were estimated from the average of each of the four data sets (generalization/transfer; end point/full feedback) and were allowed to vary to find the ideal values for the average. For each of the three different delays, we allowed subsets of the parameters to vary, fixing the others to the estimated values found over the average. This process was repeated using the single Gaussian model with various subsets of three free parameters (k, σ, and c). The lowest AIC value signifies the best fit model and a value of 2 AIC units is considered significant.

3.3: Results

3.3.1: Learning Curves

Similar to the results of the temporal decay experiment (Section 2.3.1 – Figure 2;) we observed an exponential learning curve (Figure 5) with a rapid adaptation increase during early learning and a plateau after ~50 trials. When comparing the endpoint only and full feedback conditions, there was no significant difference in learning between groups ($t.ratio = -0.31, P_{EPF/FF} > 0.75$). In both conditions, there was a significant increase ($P_{FF}, P_{EPF} < 0.0001$) in the adaptation percentage from early training (FF: 19.7 ± 1.8% EPF: 22.6 ± 2.9%) to late training (FF: 97.2 ± 3.4% EPF: 93.5 ± 1.6%). These results, in agreement with the findings presented Section

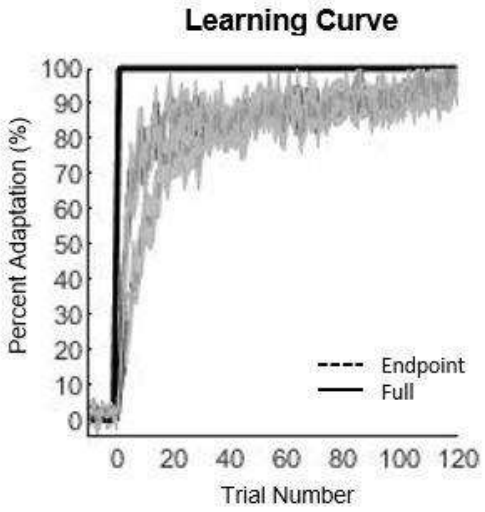

Figure 5: Learning curves during training for the intra-limb generalization experiment. The solid black line represents mean percent adaptation of all participants in the full feedback group for each trial number. The dashed black line represents mean percent adaptation of all participants in the endpoint feedback group for each trial number. The gray shaded area represents the standard error. The black step function represents the magnitude of the perturbation.

2.3.1, suggest that motor adaptation in the trained visuomotor rotation is independent of feedback type.

3.3.2: Adaptation Generalization Model

Subjects were trained to make modified reaching movements in response to a 30° visual perturbation. Each subject experienced the perturbation in one direction (clockwise or counterclockwise) and for one type of visual feedback (full feedback or end-point only). Blank (no-visual feedback) trials were implemented to establish learning retention. Based on these trials, we determined the angular deviation of the reaching movement from 0° and compared this to the last trials of the training block (for a full description of the methods see section 3.2). When tasked with replicating reach movements learned in the 0° direction to 19 different target locations spanning ±135° (Figure 2C), subjects in both feedback groups demonstrated high levels of adaptation generalization when presented with target locations most similar to the trained direction (average adaptation generalization at 0° = 85.34 ± 1.75% and at ±15° = 61.67 ± 3.12%). This generalization fell off the more the required reach angle deviated from training conditions (average adaptation generalization at ±135° = 23.16 ± 5.92%). The relationship between this adaptation generalization and angular deviation of the end target from the trained target was best represented by a modified two-Gaussian fit (Figure 6).

To examine the effect of the time delay on the spatial generalization of motor adaptation in response to the feedback perturbation, we utilized an iterative retraining protocol in which 6 consecutive blank probe trials were followed by 5-7 retraining trials (Figure 2D). Based on the completion time of one block of these probe trials (25-35 seconds) we established three temporal decay periods (4.4 ± 1.6, 12.0 ± 4.2, 24.6 ± 8.6 s). Based on the probe trials within each range, we established the percent of spatial generalization retained for the period. We fit this data with both a two-component Gaussian model and a one-component Gaussian model with varied subsets of free parameters, and used the AIC to determine the best fit model following each delay.

The AIC calculations (Table 1) indicated that the best fit model across all delay periods for the endpoint feedback condition and for the longest delay period in the full feedback condition was a two-Gaussian with four fixed parameters ($k_2,\ \sigma_1, \sigma_2, c$) and one free parameter (k_1). For the two shorter delay periods in the full feedback condition, the best fit model was indicated as a two-Gaussian with four fixed parameters ($k_1,\ \sigma_1, \sigma_2, c$) and one free parameter (k_2). However, this difference in modelling was not significant (Delay 1 $AIC_{k_2} - AIC_{k_1} = -0.33$; Delay 2 $AIC_{k_2} - AIC_{k_1} = -1.59$). In both models, the single parameter influenced by time was the magnitude of one local component (k_1, k_2). For consistency in our modelling, we used a two-Gaussian with the magnitude of the first local component (k_1) as the free parameter, holding the remainder of the values constant at the average for the feedback condition ($k_{2,FF} = 0.3\%,\ \sigma_{1,FF} = 9.8°,\ \sigma_{2,FF} = 37.1°,\ c_{FF} = 0.3\%$; $k_{2,EPF} = 0.3\%$, $\sigma_{1,EPF} = 7.8°,\ \sigma_{2EPF} = 33.3°,\ c_{EPF} = 0.3\%$) (Figure 6). This model was a significant representation for the data in both feedback conditions across all delay periods ($r^2 \geq 0.94$ for all). The local magnitude decayed across the three time ranges (Δt = 4.4±1.6s, 12.0±4.2s, and 24.6±8.6s) distinguished within the generalization probe period. These results suggest that the global adaptation was relatively unaffected by the passage of time where as the magnitude of adaptation generalization localized around the trained movement direction decreased temporally.

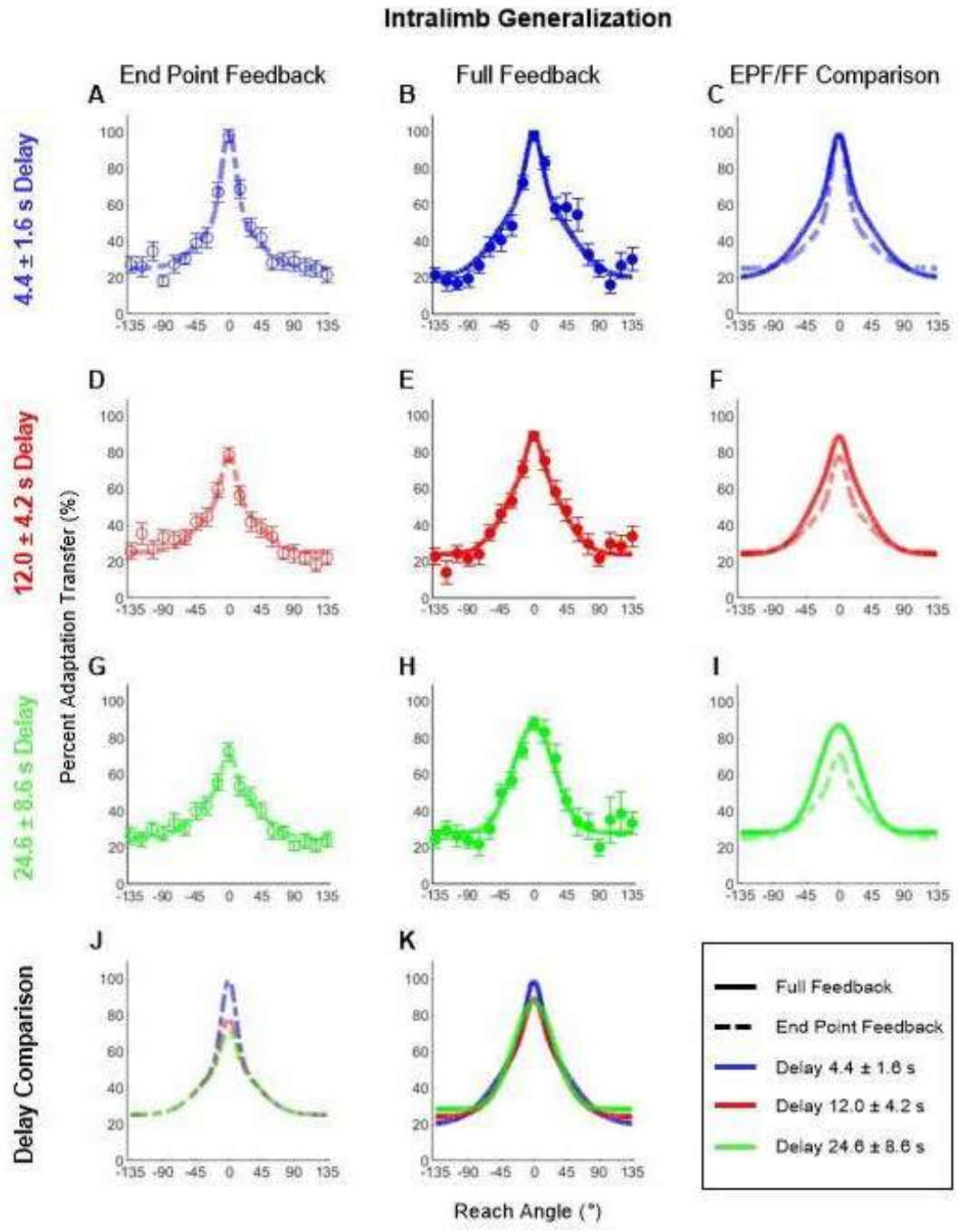

Figure 6: The influence of temporal delay on the spatial generalization of visuomotor adaptation. The dashed lines represent the best fit two-component gaussian model for the mean percent adaptation generalization of participants in the endpoint feedback group. The solid lines represent that for participants in the full feedback condition. Each color represents a different mean delay point. Plots *C, F,* and *I* depict a comparison of feedback conditions for each delay period (*C*, 4.4 ± 1.6s; *F,* 12.0 ± 4.2s; *I*, 24.6 ± 8.6s). Plots *J* and *K* show the comparison of each time point within the same feedback condition (*J*, Endpoint Feedback; *K,* Full Feedback).

Free Parameters	Generalization EPF			Generalization FF		
	Delay 1	Delay 2	Delay 3	Delay 1	Delay 2	Delay 3
Two Gaussian (5 free)	-108.77	-105.32	-118.72	-86.77	-106.52	-118
k1, sigma1, k2, sigma2	-112.96	-109.65	-122.9	-91.1	-110.7	-122.38
k1, sigma1, k2, offset	-112.62	-109.14	-123.1	-91.11	-110.53	-122.38
k1, sigma1, sigma2, offset	-108.12	-104.14	-113.17	-90.67	-98.26	-103.84
k1, k2, sigma2, offset	-79.3	-82.07	-82.38	-64.25	-75.78	-76.85
sigma1, k2, sigma2, offset	-61.74	-69.72	-71.89	-58.36	-69.84	-71.8
k1, sigma1, k2	-116.38	-112.7	-126.5	-94.85	-114.28	-126.13
k1, sigma1, sigma2	-110.95	-107.86	-116.6	-94.37	-101.87	-107.5
k1, k2, sigma2	-74.67	-76.1	-77.4	-60.37	-72.35	-72.03
sigma1, k2, sigma2	-57.69	-63.84	-66.44	-54.17	-66.13	-66.69
k1, k2, offset	-116.3	-112.8	-126.37	-94.13	-112.51	-125.84
k1, k2, offset	-115.32	-112.89	-125.48	-94.86	-113.45	-124.89
sigma1, k2, offset	-100.93	-106.48	-113.13	-93.22	-109.78	-120.07
k1, sigma2, offset	-115.63	-112.84	-125.77	-93.76	-112.93	-123.61
sigma1, sigma2, offset	-91.89	-106.15	-113.61	-86.52	-108.94	-117.4
k2, sigma2, offset	-114.56	-113.34	-120.74	-93.65	-112.94	-122.28
k1, sigma1	-119.52	-115.96	-129.59	-96.77	-114.56	-128.8
k1, sigma2	-118.51	-116.04	-128.55	-96.85	-116.15	-126.73
k1, k2	-118.52	-115.92	-128.61	-98.1	-116.61	-128.14
k2, sigma2	-117.08	-116.55	-123.07	-96.75	-116.1	-125.45
sigma1, sigma2	-91.29	-109.25	-116.37	-87.67	-111.86	-119.49
sigma1, k2	-103.14	-109.71	-116.35	-96.43	-112.95	-123.26
k1, offset	-118.37	-115.93	-128.73	-96.88	-115.76	-126.84
sigma1, offset	-93.59	-109.4	-116.38	-89.69	-112.14	-120.41
k2, offset	-110.67	-115.65	-120.91	-96.17	-116.11	-124.17
sigma2, offset	-75.85	-82.75	-82.69	-67.17	-77.85	-78.72
k1	**-121.21**	**-118.73**	**-131.4**	-98.68	-117.34	**-129.13**
sigma1	-94.12	-111.69	-119.17	-89.64	-113.67	-122.15
k2	-112.85	-118.08	-123.66	**-99.01**	**-118.93**	-126.81
sigma2	-69.04	-76.36	-78.33	-61.11	-74.55	-74.66
offset	-107.01	-117.02	-119.37	-94.06	-115.98	-120.63
Single Gaussian (3 free)	-101.9	-101.08	-112.71	-86.28	-106.25	-113.82
k sigma	-104.93	-104.31	-114.93	-89.37	-109.48	-116.82
k offset	-102.04	-104.26	-112.33	-89.18	-109.46	-115.44
sigma offset	-67.22	-76.73	-78.56	-62.06	-76.53	-78.67
offset	-96.95	-106.64	-112.18	-80.04	-109.05	-115.96
sigma	-63.8	-72.97	-75.94	-57.29	-72.94	-73.91
k	-104.63	-106.93	-115.16	-92.03	-112.19	-118.24

Table 1: AIC Matrix comparing the goodness of fit for each Gaussian model. The AIC function balances the maximum likelihood estimate and the number of independent variables to determine which model best explains variation in the data with the fewest variables. Each iteration is holding constant one or more model parameters at the best fit value for the average data. The best fit model is represented by the lowest (most negative) AIC value (highlighted). Across all conditions, the best fit model is a two Gaussian with 4 fixed parameters ($k_2, \sigma_1, \sigma_2, c$; $k_1, \sigma_1, \sigma_2, c$) and one free parameter ($k_1; k_2$) for all EPF/FF delay 3, and FF delay 1/2 respectively. For consistency, we used the two-Gaussian fit with free parameter k_1 (bold).

Chapter 4: Spatiotemporal Properties of Inter-limb Transfer of Visuomotor Adaptation

4.1: Abstract

The transfer of motor learning between limbs (i.e., tasking the untrained left limb with a behavior trained on the right limb) results in the loss of some visuospatial refinement of the adaptation. This chapter compares the effects of different forms of feedback (provided throughout movement or restricted to only the endpoint) on the spatiotemporal relationships for inter-limb transfer. In the task, subjects moved a screen cursor to a peripheral target and a rotation was applied to the visual feedback of the unseen hand motion. The transfer of adaptation was assessed at 19 different locations (spaced 15° apart, symmetric around the trained direction) and examined following three delays (approximately 4, 12, and 25 s). Adaptation transfer was best represented by a single Gaussian model. Modelling results showed that the spatiotemporal patterns of inter-limb transfer remained near constant across time for both types of feedback.

4.2: Methods

Participants

Forty healthy participants recruited from the George Mason University population participated in this study. All participants were right-handed. The demographics (e.g., age, gender, etc.) were representative of the University population. Participants used both dominant and non-dominant hands during the task. Each subject completed only one condition of the experiment. This research was approved by the George Mason University Institutional Review Board and all participants gave informed consent.

Experimental Setup and Procedure

The details of the experimental setup are the same as described in section 2.2. Aligned with the Intra-limb Generalization Experiment (outlined in section 3.2), this task was designed to determine the feedback dependency of the spatial characteristics of the between-limb transfer of visuomotor learning. In accordance with the flow diagram in Figure 2D, subjects underwent the same baseline and training blocks as in our previous task. Participants were randomly selected to undergo one of the two feedback conditions: full visual feedback (n=20) and endpoint visual feedback (n=20); and receive one of two rotational perturbation conditions: $\theta = +30°$ or $\theta = -30°$. Upon completing the training block, subjects began the skill retention block which consisted of 6 transfer probe trials followed by 5-7 retraining trials. In the transfer probe trials for this task, subjects were tasked with completing movements to pseudo-randomly selected target locations using their left hands in the absence of visual feedback (blank trials). After the 6 skill transfer probe trials, subjects underwent 5-7 retraining trials using their right hands with their assigned visual feedback condition. This process of 6 probe trials followed by 5-7 retraining trials was repeated such that each of the 19 movement directions was tested in each of the 6 different placements within the probe sequence. This yielded a total of 209-247 movements for each subject between the three blocks.

Analysis

For each reaching movement, the movement angle and percent adaptation were calculated as described in section 2.2.4. For probe trials, subject performance was evaluated based on how well subjects maintained adaptation following the experimental condition. The percent adaptation transfer was determined by finding the ratio of movement angle to target location angle for reaching movements using the untrained limb and comparing this to the percent adaptation of the trained limb at the end of training.

Computational Modelling

A single Gaussian model was applied to provide a general representation of the changes in the spatial relationships across the different conditions in the inter-limb experiments. The single Gaussian model:

$$z(\theta) = ke^{-\frac{|\theta-\theta_0|^2}{2\sigma^2}} + c$$

is representative of the amount of adaptation transfer (z) to reaching movements utilizing the untrained limb to various target locations (θ). As with the two-component model, the single Gaussian provides insight into the localization/globalization of motor learning. The magnitude (k) and width (σ) of the transfer function at the peak movement direction (θ_0) are localized to the given target location whereas the offset (c) demonstrates the global transfer of adaptation to all target locations.

Statistics

Similar to the generalization experiment (section 3.2), data were analyzed offline using Matlab 2019a (The MathWorks, Natick, MA) and R 3.6.2 (r-project.org). Trials that had very slow/fast movement speeds (peak speed < 0.2 m/s or > 0.5 m/s) were excluded (~9% of total trials for full feedback group and ~11% of total trials for endpoint feedback group). We tested the main effect of group (full feedback and endpoint feedback) on the amount of adaptation with a linear mixed effects model (LMM) in R using the lmerTest package (Kuznetsova et al. 2014) with the fixed effects of group (full feedback and endpoint feedback) and period (different trial periods in the experiment, e.g., early learning and late learning period; first 10% and last 10% of training trials, respectively) and random effect of subjects. The model was estimated using the restricted maximum likelihood method (REML) and the significance was obtained using Kenward-Roger and Satterhwaite's approximations with pbkrtest package (Halekoh et al. 2014). If significance was identified, post hoc tests were performed using the emmeans package and adjusted for multiple comparisons using Bonferroni-Holm corrections. Effect size (d) was calculated using Cohen's d (Cohen 1988) measurement (for LMM analysis, generalized effect size was computed

following similar procedures of Cohen's d measurement using the eff_size function in the emmeans package). For all tests, the significance level was set to 0.05. In all cases, group data are presented as mean±SEM and estimation of the proposed model coefficients were reported with 95% confidence intervals.

To quantify the goodness of fit for the adaptation transfer model described above, we fit the function with different subsets of free parameters and computed the Akaike information criterion (AIC) for each model (Akaike 1974). Similar to the generalization experiment (Section 3.2), the percent adaptation transfer data was fit with both a two-Gaussian model (see 3.2) and a single Gaussian model. The peak movement direction (θ_0) was set to the trained movement direction. In the case of the two-Gaussian model, the five parameters (k_1, k_2, σ_1, σ_2, and c) were estimated from the average of each of the visual feedback conditions (end point/full feedback) and were allowed to vary to determine the ideal values for the average. For each of the three different delays, we allowed subsets of the parameters to vary, fixing the others to the estimated values found over the average. This process was repeated using the single Gaussian model with various subsets of three free parameters (k, σ, and c). The lowest AIC value signifies the best fit model and a value of 2 AIC units is considered significant.

4.3: Results

4.3.1: Learning Curves

Similar to the results of the temporal decay and intra-limb generalization experiments (Section 2.3.1 – Figure ; Section 3.3.1 – Figure 4) we observed an exponential learning curve (Figure 7) with a rapid adaptation increase during early learning and a plateau after ~50 trials. When comparing the endpoint only and full feedback conditions, there was no significant difference in learning between groups (early: $P_{EPF/FF} > 0.53$ late: $P_{EPF/FF} > 0.28$). In both conditions, there was a significant increase (P_{FF}, $P_{EPF} < 0.01$) in the adaptation percentage from early training (FF: 20.1 ± 2.3% EPF: 19.4 ± 1.6%) to late training (FF: 93.7 ± 1.2% EPF: 92.1 ± 1.4%). These results, in agreement with the findings presented Sections 2.3.1 and 3.3.1, suggest that motor adaptation in the trained visuomotor rotation is independent of feedback type.

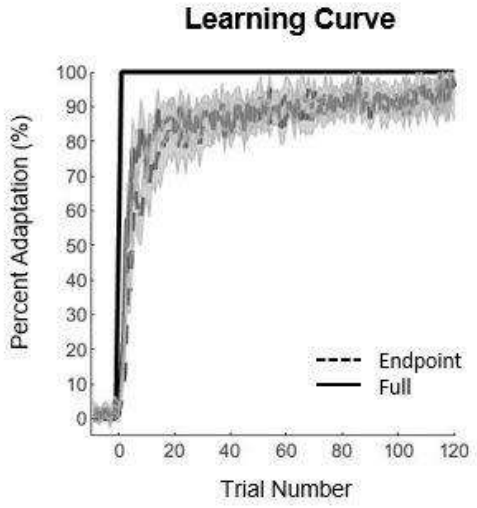

Figure 7: Learning curves during training for inter-limb transfer experiment. The solid black line represents mean percent adaptation of all participants in the full feedback group for each trial number. The dashed black line represents mean percent adaptation of all participants in the endpoint feedback group. Solid step function represents the relative magnitude of the perturbation.

4.3.2: Adaptation Transfer Curves

Subjects were trained to make modified reaching movements in response to a 30° visual feedback perturbation. Each subject experienced the perturbation in only one direction (clockwise or counterclockwise) and only one type of visual feedback (full feedback or end-point only). Blank (no-visual feedback) trials were implemented to establish learning transfer. Based on these trials, we determined the angular deviation of the reaching movement from 0° and compared this to that of the last trials of the training block (for a full description of the methods see section 3.2). When

tasked with replicating reach movements learned in the 0° direction to 19 different target locations spanning ±135° (Figure 2C) using the untrained limb, subjects in both feedback groups demonstrated moderate levels of adaptation transfer when presented with target locations most similar to the trained direction (average adaptation generalization at 0° = 25.82 ± 1.72% and at ±15° = 24.17 ± 4.33%). This generalization fell off the more the required reach angle deviated from training conditions (average adaptation generalization at ±135° = 12.42± 2.92%). The relationship between this adaptation transfer and angular distance between the probe target and the trained target was best represented by a single Gaussian model (Figure 8).

To examine the effect of the time delay on the inter-limb transfer of motor adaptation in response to the feedback perturbation, we utilized an iterative retraining protocol in which 6 consecutive blank probe trials on the untrained limb were followed by 5-7 retraining trials on the trained limb (Figure 2D). Based on the completion time of one block of these probe trials (25-35 seconds) we established three temporal decay periods (4.4 ± 1.3, 11.8 ± 3.0, 25.7 ± 8.3 s). Based on the probe trials within each range, we established the percent of spatial generalization retained for the period. We fit this data with both a two-component Gaussian model and a one-component Gaussian model with varied subsets of free parameters and used the AIC to determine the best fit model following each delay. The AIC calculations indicated varying best fit models across the delay points in both full and end point feedback conditions (Table 2). In three of the six conditions (EPF delay 3, FF delays 1 and 3) the best fit model was indicated as a single Gaussian with two fixed parameters (*σ, c)* and one free parameter (*k)*. In both feedback conditions at the second delay period, the best fit was indicated to be a two-Gaussian with the global offset as the only free parameter. In the EPF delay 1 condition, the best fit model was indicated to be a two-Gaussian with the only free parameter as a single local magnitude (k_2). However, these models were not significantly better fits than the one Gaussian with the single free parameter, *k* (EPF Delay 1 $AIC_{k_2} - AIC_k = -0.63$; EPF Delay 2 $AIC_c - AIC_k = -0.51$; FF Delay 2 $AIC_c - AIC_k = -0.83$). To consistently assess temporal and visual feedback influence on the inter-limb transfer of motor

learning, we applied the best fit model with the fewest parameters: the single Gaussian fit in which the only parameter varying with time was the magnitude (*k*), holding the remainder of the values constant at the average for the feedback condition ($\sigma_{FF} = 34.3°$, $c_{FF} = 0.1\%;$, $\sigma_{EPF} = 29.4°$, $c_{EPF} = 0.1\%$). This model was a significant representation for the data in both feedback conditions across all delay periods ($r^2 \geq 0.92$ for all). The local magnitude decayed across the three time ranges (Δt = 4.4±1.3s, 11.8±3.0s, and 25.7±8.3s) distinguished within the generalization probe period. These results suggest that the global transfer was relatively unaffected by the passage of time whereas the magnitude of adaptation transfer localized around the trained movement direction decreased temporally.

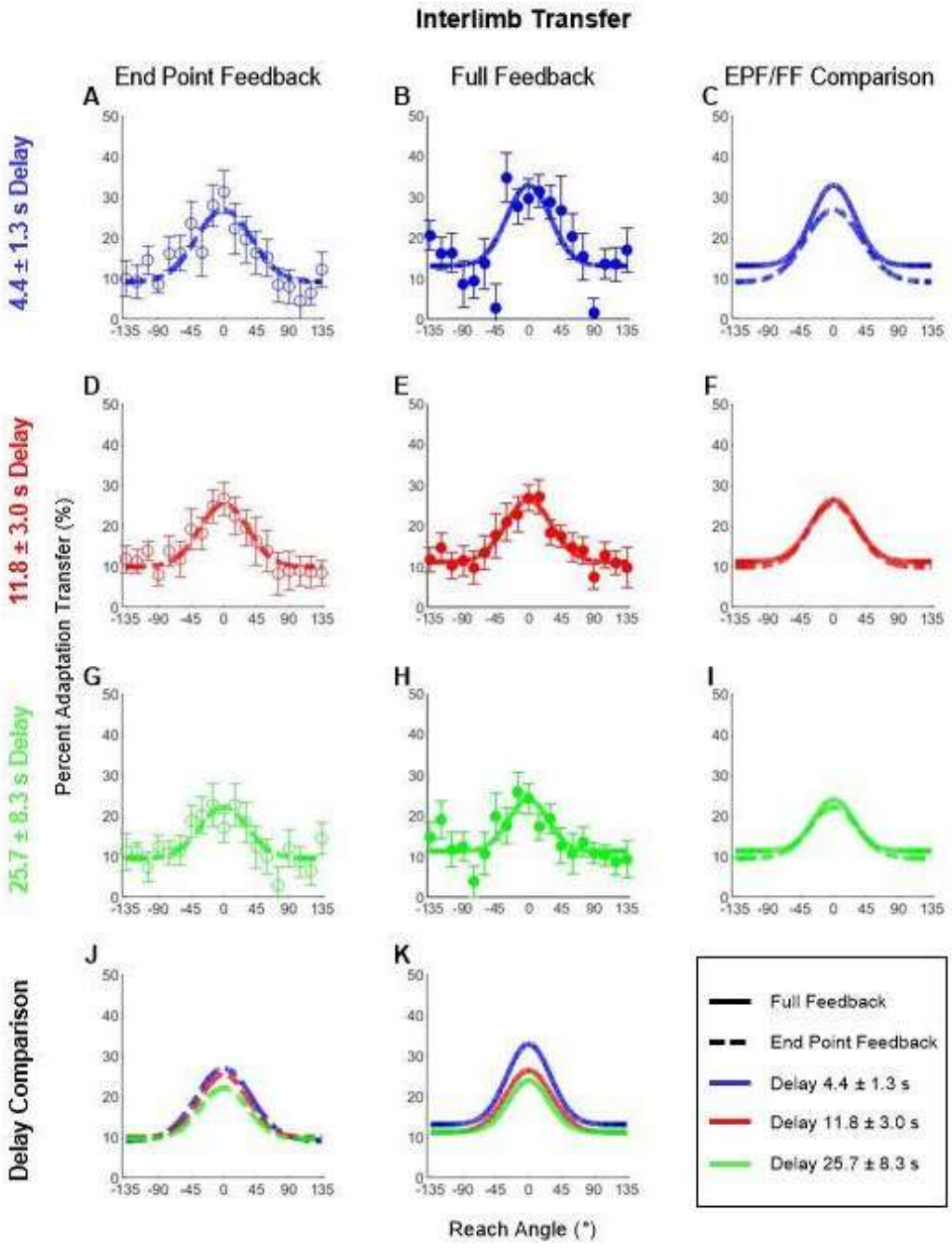

Figure 8: Influence of temporal delay on the inter-limb transfer of visuomotor adaptation. The dashed lines represent the best fit single-component Gaussian model for the mean percent adaptation generalization for participants in the endpoint feedback group. The solid lines represent the participants in the full feedback condition. Each color represents a different mean delay point. Plots *C, F,* and *I* depict a comparison of feedback conditions for each delay period (*C*, 4.4 ± 1.3s; *F,* 11.8 ± 3.0s; *I*, 25.7 ± 8.3s). Plots *J* and *K* show the comparison of each time point within the same feedback condition (*J*, Endpoint Feedback; *K,* Full Feedback).

Free Parameters	Transfer EPF			Transfer FF		
	Delay 1	Delay 2	Delay 3	Delay 1	Delay 2	Delay 3
Two Gaussian (5 free)	-112.89	-132.16	-113.33	-86.05	-134.05	-109.21
k1, sigma1, k2, sigma2	-65.56	-66.07	-63.16	-68.70	-69.10	-66.30
k1, sigma1, k2, offset	-115.61	-136.55	-117.71	-90.43	-137.68	-113.48
k1, sigma1, sigma2, offset	-112.35	-118.37	-99.23	-84.65	-114.74	-103.87
k1, k2, sigma2, offset	-101.11	-110.50	-102.39	-77.53	-100.38	-99.84
sigma1, k2, sigma2, offset	-92.08	-99.57	-97.36	-77.53	-100.38	-99.84
k1, sigma1, k2	-119.33	-140.13	-121.47	-93.71	-140.54	-116.74
k1, sigma1, sigma2	-115.67	-122.12	-102.99	-88.16	-117.76	-107.48
k1, k2, sigma2	-98.42	-105.55	-101.87	-74.85	-98.84	-101.08
sigma1, k2, sigma2	-87.58	-93.49	-94.76	-74.85	-98.84	-101.08
k1, k2, offset	-119.27	-140.23	-120.05	-94.19	-141.28	-115.04
k1, k2, offset	-118.89	-140.21	-121.28	-94.19	-141.44	-117.24
sigma1, k2, offset	-118.08	-139.80	-120.19	-94.19	-141.44	-117.17
k1, sigma2, offset	-120.69	-140.06	-120.44	-93.38	-141.54	-115.72
sigma1, sigma2, offset	-116.70	-139.80	-118.98	-93.38	-141.54	-115.72
k2, sigma2, offset	-118.24	-139.87	-120.71	-94.19	-141.83	-117.34
k1, sigma1	-122.27	-143.38	-121.75	-97.04	-142.31	-114.74
k1, sigma2	-123.23	-143.25	-123.45	-95.42	-142.78	-118.05
k1, k2	-122.07	-143.26	-124.48	-96.96	-143.76	-119.99
k2, sigma2	-121.35	-142.95	-123.97	-97.10	-143.73	-120.32
sigma1, sigma2	-119.85	-142.61	-121.90	-95.34	-142.78	-118.05
sigma1, k2	-121.33	-143.00	-123.41	-96.96	-143.73	-119.87
k1, offset	-122.14	-143.30	-123.30	-96.59	-144.54	-118.30
sigma1, offset	-119.63	-142.94	-121.96	-96.59	-144.54	-118.30
k2, offset	-121.17	-143.02	-123.88	-97.45	-144.69	-120.43
sigma2, offset	-99.61	-107.08	-100.80	-84.36	-106.83	-105.75
k1	-121.98	-143.23	-121.75	-94.39	-142.31	-114.74
sigma1	-121.33	-145.41	-123.18	-97.17	-145.16	-117.59
k2	**-124.02**	-145.79	-126.71	-99.81	-146.58	-122.72
sigma2	-93.57	-100.23	-99.80	-80.92	-104.91	-106.75
offset	-122.61	**-145.85**	-124.91	-99.44	**-147.39**	-121.15
Single Gaussian (3 free)	-109.46	-131.28	-113.33	-86.05	-133.69	-109.20
k sigma	-120.73	-142.50	-124.73	-97.10	-143.71	-120.31
k offset	-120.54	-142.57	-124.65	-97.45	-144.67	-120.44
sigma offset	-99.00	-106.38	-100.48	-84.36	-106.82	-105.74
Offset	-122.05	-145.40	-125.62	-99.44	-147.36	-121.15
sigma	-93.08	-99.68	-99.46	-80.93	-104.93	-106.76
k	-123.39	-145.34	**-127.46**	**-99.81**	-146.56	**-122.72**

Table 2: AIC Matrix comparing the goodness of fit for each Gaussian model The AIC function balances the maximum likelihood estimate and the number of independent variables to determine which model best explains variation in the data with the fewest variables. A value of 2 AIC units is considered statistically significant. Each iteration is holding constant one or more model parameters at the best fit value for the average data. The best fit model is represented by the lowest (most negative) AIC value (bold). As shown above, the best fit varied across conditions. For consistency, we selected the model with the best fit and fewest parameters - the single Gaussian with one free parameter (k) (highlighted) - as the model for this task. This model was not significantly different from the best fit in any condition.

Chapter 5: An Investigation of Distributed Bimanual Coordination

5.1: Abstract

Bimanual control of the upper limbs (i.e., the coordination of movements between the two arms) typically involves an unequal distribution of control between the limbs (e.g., hammering a nail, one hand steadies the nail while the other controls the hammer). Although there is a growing literature on the processes involved when humans learn new motor patterns using one limb, there is a substantial gap in the understanding of how the two hands coordinate control in accomplishing a single task when faced with external perturbations. Importantly, this gap includes relating quantitative behavioral measures to the neural activation patterns that underlie bimanual control and computational models that depict this behavior. This chapter will present preliminary data supporting a novel bimanual adaptation paradigm for future study in conjunction with neural imaging techniques. The task involves examining the inter-manual performance during manipulations of a jointly controlled object perturbed using altered visual feedback. Trajectory mapping and coordination was examined through alignment of velocity profiles to determine the effect of varying experimental conditions on motor adaptation.

5.2: Methods

Participants

Four healthy participants (1 male and 3 females) recruited from the University of California, Davis Sensorimotor Integration Lab participated in this study. All participants were right-handed and were familiar with the KINARM robotic manipulandum. Subjects had minimal prior knowledge about the conditions of the experiment.

Experimental Setup

Participants were seated in an adjustable chair in front of a two-arm robotic manipulandum (KINARM End-Point Lab, BKIN Technologies). Chair height was adjusted accordingly so participants could comfortably rest their forehead on the system's headrest and subjects were positioned so that the center of their body aligned with the center of the workspace. Visual feedback from the task was projected onto a horizontal mirror display from a downward-facing LCD monitor positioned directly above. Participants grasped the right handle of the robotic

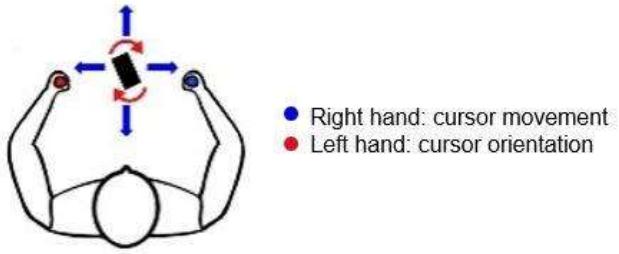

Figure 9: Joint bimanual coordination of an oriented rectangular target. The participant uses the right hand to control the cursor trajectory and left hand to control the 360° rotational orientation.

manipulandum in their right hand and a rotation knob (3.8 cm diameter) in their left hand (Figure 9). The mirror display obstructed visibility of both arms to limit feedback of upper limb position to only what was observed on the screen. Subjects were instructed to place a rectangular cursor (1 cm length, 0.5 cm width) in an oriented rectangular target (1.5 cm length, 0.75 cm width) located 12 cm from the starting position. During movements, the manipulandum recorded measurements of hand position, velocity, and cursor orientation at a sampling rate of 1000 Hz.

Experimental Procedure

This procedure was partly adapted from the work in chapters 2-4 as well as previous unimanual motor learning studies (Stewart et al. 2013; Zhou et al. 2017). Subjects (n=4) were instructed to carryout translational and rotational movements simultaneously to move the cursor

into the oriented target. Once participants grasped the handle, the KINARM applied a force to move the cursor into the starting target. Once there, the handle was locked in this position for 500 ms at which point the end target appeared on screen and the handle was released from the hold position. Subjects were instructed to wait an additional 500 ms until this end target turned from red to green. Upon reaching the target, the target turned one of three colors: green to signify optimal reaching velocity, yellow to signify that the participant did not move quickly enough, or red to signify the reaching velocity was too high. The ideal movement duration for this task was predetermined to be between 250 and 400 ms. Following each trial, the manipulandum applied a force to return the cursor to the starting position.

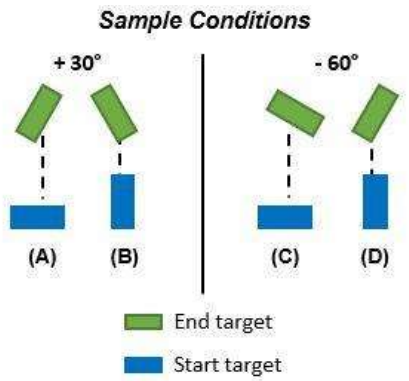

Figure 10: target orientation combinations analyzed for results. Participants were presented with 2 possible cursor start orientations and 6 possible end orientations. *A* and *B* depict a -30° rotation requirement from the starting orientation (*A* – horizontal; *B* – vertical) to the target orientation. *C* and *D* show a +60° rotation requirement.

Participants moved through three experimental blocks in which there were two possible starting orientations (horizontal and vertical) and six possible end target orientations (0°, 30°, 60°, 90°, 120°, and 150°). Each of these 12 orientation combinations was presented eight times in a randomized order for a total of 96 trials in each block. During the baseline block, subjects received visual feedback that directly corresponded to the position of the reaching hand. In the subsequent training block, a visuomotor gain was applied such that the participant was required to move 25% further to reach the target (12 cm target distance required 16 cm reaching movement). Following the 96 training sessions, subjects entered the decay block in which the visual feedback conditions reverted to those of the baseline block.

To assess learning, we observed several parameters to quantify inter-limb coordination and bimanual performance. Among these were the cursor rotation over relative distance calculated as:

$$\mathbf{d_{rel}} = \frac{\mathbf{y_{cursor}} - \mathbf{y_{start}}}{\mathbf{y_{target}}}$$

and relative time:

$$\mathbf{t_{rel}} = \frac{\mathbf{t_{elapsed}}}{\mathbf{t_{start} - t_{end}}} \mathbf{x\ 100}$$

For the purposes of this preliminary assessment, we primarily focused on qualitative assessments for four experimental conditions: rotational gains of +30° and -60° from both the horizontal and vertical starting orientations (Figure 10).

5.3: Results

5.3.1 Performance

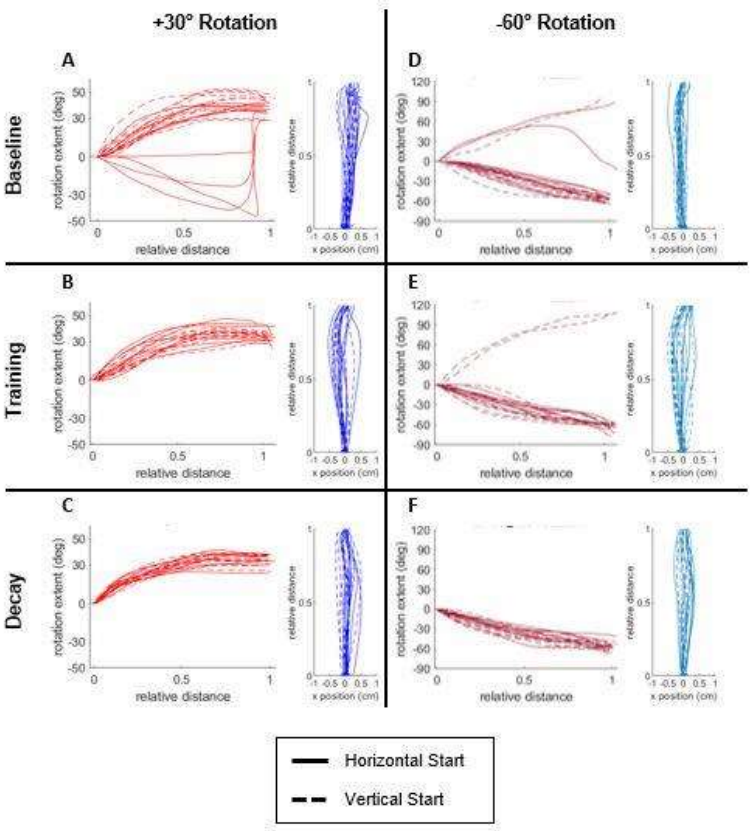

Figure 11: cursor trajectory and rotation plotted along reaching path for the three experimental blocks. *A-C* depict the trajectory and rotation in the +30° condition (See Fig. 10 *A-B*) *D-F* reflect the -60° condition (Fig. 10 *C-D*). Red plots show the rotation extent plotted over the relative y distance. Blue plots show the corresponding reach trajectories (x-axis) over the same relative distance (y-axis).

The combined adaptation between the two limbs was observed by manipulating the gain for the right hand (translational cursor movement) and assessing compensation in the left hand

(cursor orientation). To accomplish the desired target orientation, subjects could rotate the cursor +30° (optimal) or -150° in the +30° condition, and -60° (optimal) or +120° in the -60° condition. Subjects achieved nearly ideal rotation curves (red) for the +30° and -60° cases during the decay block as depicted in Figures 10 C and 10 F respectively. These curves show rotation to the desired extent (final angle) in the optimal direction (rotation trajectory) with consistency across the movement distance (curve smoothness). There are fewer rotational deviations and in-trial corrections shown in Figure 10 D than 10 A, indicating that subjects exhibited a faster initial learning in the -60° rotation case and performed better from a vertical start target. However, in the training block, there were fewer in-trial corrections and more rotations in the optimal direction for the +30° condition than the -60° condition (Figure 11 B, E). This suggests that learning retention was greater in the +30° case regardless of start condition. Overall, rotation was more consistent across trials from a vertical start target than those from a horizontal start target. Cursor trajectories along the x axis were consistent across baseline and decay blocks and deviated to the left in the training block.

5.3.2 Coordination

The coordination of the two limbs (overlap of rotational and reaching movement) was assessed through the velocity profiles for both reach velocity (right limb) and orientation velocity (left limb). Subjects increased reaching velocity from early to late baseline trials (Figure 12 A).

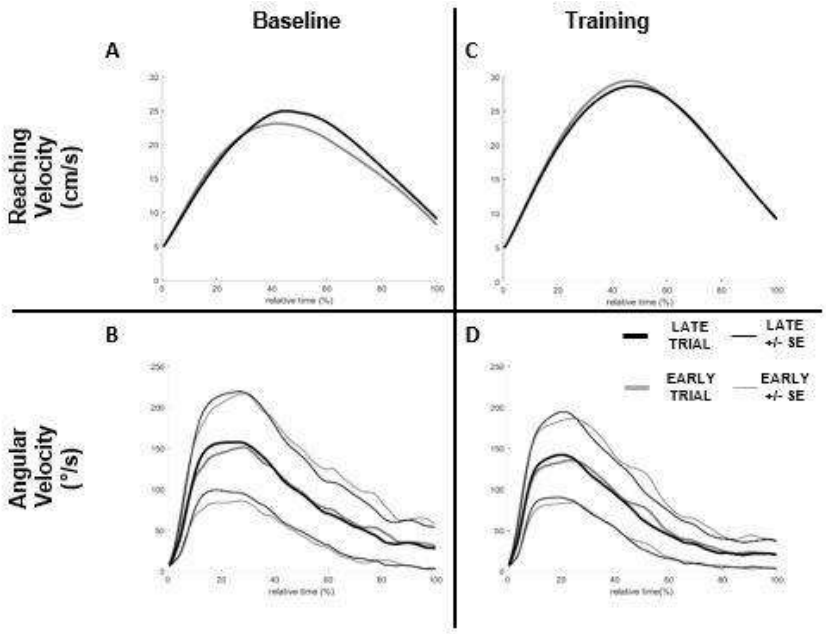

Figure 12: Velocity profiles for reaching motion and angular rotation over relative time. *A-B* show the reach velocity and angular velocity respectively for the baseline block averaged across all participants in all conditions. *C-D* show the same information for the training block. The thick gray line represents the mean over the early trials and the black line represents the mean over the late trials. The thin gray and black lines represent ± 1 SE for the early and late trials respectively.

Reaching velocity was maintained across training trials, demonstrating retention (Figure 12 C). Subjects maintained the same angular velocity profile from baseline to training blocks, peaking at approximately 20% of the movement duration and steadily decreasing for the remainder. (Figure 12 B, D).

These results demonstrate that the angular difference between the start orientation and the target orientation influenced the ability to learn the required movement coordination pattern. The consistency of the velocity profiles over the relative task completion time in Figure 12 suggests that with the applied gain decrease, subjects increased the duration of object rotation to match the longer movement duration. In the decay block (Figure 11 C, F), all rotations were in the optimal direction with minimal need for in-trial correction. In the baseline block (Figure 11 A, D), there were several rotations in the suboptimal direction (-150°/+120°), multiple trials with in-trial corrections, and little consistency across trials. Thus, when comparing motor performance in the decay block to that in the baseline block, subjects demonstrated the ability to revert to the optimal movement patterns in fewer trials than the initial learning in the baseline block.

Chapter 6: Discussion and Future Aims

6.1: Discussion

The experiments outlined in chapters 2-4 provide a comprehensive quantification and comparison of the spatiotemporal properties of unimanual intra-limb generalization and inter-limb transfer. **Chapter 2** established that the temporal stability of the motor learning in response to the rotational feedback perturbation is independent of the type (full vs. endpoint). **Chapter 3** further investigated the temporal decay in the context of spatial generalization; we found that this was best represented by a two-component Gaussian model with only a single local magnitude temporally modulated, independent of the feedback condition. **Chapter 4** expanded on these findings, determining the best fit model for inter-limb transfer as a single-component Gaussian, unaffected by the passage of time or feedback type. **Chapter 5** outlined a proposed method for studying similar aspects within a bimanual coordination framework and provided preliminary data supporting its potential. This discussion will link the results of the previous chapters and postulate the significance of the findings.

Different models capture the spatiotemporal patterns of intra-limb generalization and inter-limb transfer

Based on the behavioral results and the AIC analysis in chapters 3 and 4, the best fit model of intra-limb generalization was a two-component Gaussian model, whereas a one Gaussian fit best represented inter-limb transfer. We hypothesize that this may be due to the differing neural requirements of these two tasks. Previous studies have proposed theoretical neural pathways underlying motor learning. Intra-limb generalization is thought to involve intra-hemispheric neural tuning changes from adaptation, resulting in a more refined sensorimotor mapping to various directions and thus recognizable local and global components (deXrivy et al.

2011; Shadmehr and Moussavi 2000). In contrast, inter-limb transfer of learning requires neural communication across hemispheres, resulting in a more broadly generalized sensorimotor map (Sainburg and Wang 2002; Shadmehr 2004). This may explain the loss of the local components of adaptation seen in our inter-limb transfer model.

Furthermore, this difference between models may point to the difference in implicit and explicit learning. Implicit learning mechanisms are driven by a sensory-prediction error and are thought to occur within specific end-effectors (e.g. wrist/elbow joints) whereas explicit learning is driven by target error and so takes place in conscious efforts (Poh et al. 2016; Taylor et al 2014). This type of learning is more broadly applicable, exceeding the trained end-effector, and extending to variable circumstances. It is possible that the spatiotemporal model for inter-limb generalization is equally influenced by both implicit and explicit learning mechanisms – resulting in the two-component Gaussian model – whereas the transfer of adaptation relies more heavily on the explicit learning achieved during the training block – resulting in a lower resolution spatiotemporal map and a one-Gaussian model. This is further implied by the fact that implicitly learned behaviors are more temporally influenced – learning both increases and decays systematically as a function of time – whereas explicit learning is more motion dependent – learning progresses more sporadically prior to behavior stabilization (Bindra et al. 2021; Poh et al. 2016; Bond and Taylor 2015).

The AIC calculations also demonstrated that the majority (generalization: $k_2, \sigma_1, \sigma_2, c$; transfer: σ, c) of the model parameters are temporally stable, with only the local magnitude (k_1) changing with time in the intra-limb generalization for both feedback conditions and the magnitude (k) changing with time in both conditions of the inter-limb transfer experiment. This suggests that the local magnitude is learned implicitly. This temporal dependence suggests that the local magnitude is learned implicitly. In the intra-limb generalization experiment, there is a greater temporal decay in the local magnitude than in the inter-limb transfer. The greater

temporal stability of inter-limb transfer also supports our hypothesis that adaptation transfer occurs with explicit learning.

Influence of feedback on intra-limb generalization and inter-limb transfer

Our findings suggest that the form of visual feedback (full versus endpoint) influences intra-limb generalization (Chapter 3) and inter-limb transfer (Chapter 4) differently. It has been shown that the form of feedback promotes different learning mechanisms; that is, full visual feedback promotes more explicit learning whereas end point only feedback promotes implicit learning (Taylor et al. 2014). Additionally, Bindra et al. (2021) demonstrated that implicit learning is temporally dependent while explicit learning is more temporally stable. As such, we expect that subjects receiving end point only feedback demonstrate greater skill decay over time. In the intra-limb generalization experiment, our results followed the expected results: participants receiving full visual feedback demonstrated a less temporally dependent, higher percentage of adaptation generalization when compared with those receiving endpoint feedback only (Figure 6). However, in the inter-limb transfer experiment, we observed a greater temporal dependence in the full feedback condition in the following only the first time-delay. Adaptation had a higher transfer percentage following shorter time delays which decreased so there was no difference between the two feedback groups following the two later time periods (Figure 8). These findings demonstrate the difference in learning mechanisms between the two experimental conditions (intra-limb versus inter-limb). The intra-limb experiment confirms the presence of more extrinsic learning mechanisms occurring when full visual feedback is received when compared with endpoint feedback only. The inter-limb experiment shows that the feedback condition has less effect on the transferability of learning between the two limbs. The greater temporal dependence of the full feedback case in the inter-limb experiment may suggest differing neural mechanisms at play during transfer.

Neural substrates for intra-limb generalization and inter-limb transfer

In chapters 2-4, participants developed a new sensorimotor map to compensate for the visual feedback perturbations and demonstrated the transferability of this map to varying directions within a single limb and to the untrained limb. The pattern of map retention may align with two previously proposed neural models of inter-limb transfer: **the callosal model** (Taylor and

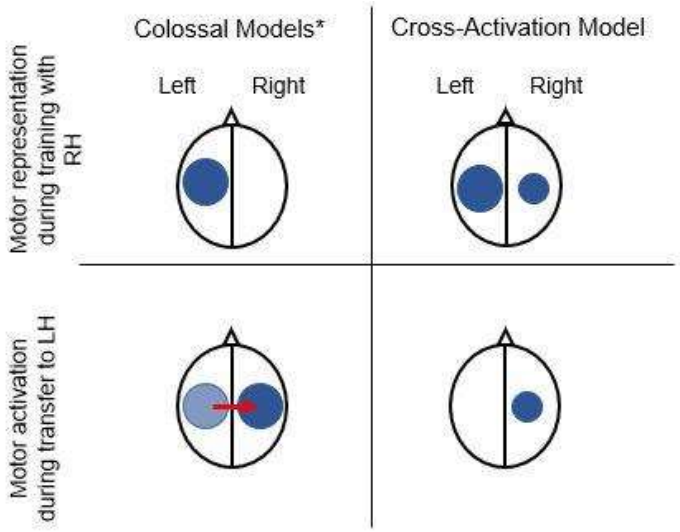

Figure 13: A diagram of two proposed neural models of interlimb transfer from right hand (RH) to left hand (LH). The top row represents neural activation during (RH) training, while the bottom row represents that upon transfer to the LH. The blue dot shows the hemispheric location of the motor programs developed/used in each condition. 'Left' and 'Right' denote the respective hemispheres. *there are two forms of the callosal (access) model: the 'original' and the 'modified'. Predictions from both are equivalent in their depiction. The callosal models both posit that at transfer, the right hemisphere gains access to the previously developed representation (note the faded dot), stored in the left hemisphere, via the corpus callosum. The cross-activation model posits that during RH adaptation, an 'inferior' version of the motor program is created in the right hemisphere (note the smaller dot), and it is this program that would be used at transfer. Adapted from Anguera et al. (2017).

Heilman 1980; Sainburg and Wang 2002) and **the cross-activation model** (Parlow and Kinsbourne 1989). The callosal model suggests that motor control is lateralized to the dominant hemisphere and must travel across the corpus callosum when applied to the non-dominant limb. The cross-activation model suggests that during training, motor learning occurs simultaneously in both hemispheres with a more complete motor program in the dominant hemisphere and an inferior motor program in the non-dominant hemisphere. Both theories are partially supported by

brain activation patterns observed using fMRI during motor learning paradigms (visuomotor rotation) involving the dominant limb and transfer to the nondominant limb (Anguera et al. 2007). In accordance with the callosal model, activation observed at transfer partially overlapped with the areas engaged during adaptation. However, in accordance with the cross-activation model, bilateral activation was observed during adaptation along with partially lateralized activation observed at transfer. This data suggests that early motor learning is highly bilateral, and transfer largely occurs in the hemisphere contralateral to the untrained limb. However, these findings may also be indicative of differences in early learning (initial rapid learning that is typically characterized by end effector precision and is not retained long-term) and late learning (learning that occurs later in training characterized by movement optimization and greater after-training retention). Activation was observed at the temporal cortex, medial frontal, and medial occipital gyri which are areas previously thought to be involved in late learning (Graydon et al 2005). Other early studies suggest that the nondominant limb is more effective at end point control but lacks the trajectory refinement of the dominant limb (Sainburg and Kalakanis 2000, Sainburg 2002). The variability of the sensorimotor map we observed may be due to some combination of the learning mechanisms characterized by these previous findings. Independent of time delay or feedback condition, we observed greater adaptation retention within generalization than across transfer. On average, subjects demonstrated a global offset of 25.02% within the intra-limb generalization experiment whereas the global offset was 10.82% during inter-limb transfer, showing a 56.75% decrease after transfer. A similar pattern was seen across the average local adaptation transfer at the trained direction. In the generalization experiment, this value was observed to be 85.34 ± 1.75% whereas in the transfer experiment we found a 25.82 ± 1.72% average transfer, showing a 69.74% loss of adaptation during transfer. This finding is in alignment with both of the previously mentioned neural models as both predict diminished performance in the untrained limb. Additionally, our results suggest that generalization is temporally dependent whereas transfer is temporally independent. These spatiotemporal characteristics are not

accounted for in previous models. It should be noted that the experiments did not account for limb dominance; all participants completed the same tasks regardless of limb dominance. As such, there may be handedness related neural impacts that are unaccounted for. Nevertheless, we have demonstrated modelling differences between intralimb generalization and interlimb transfer that suggest an avenue for studying neural substrates involved in each.

Neural substrates for bimanual motor adaptation

In chapter 5, participants acquired a novel distributed bimanual coordination movement pattern and demonstrated the effects of target orientation on motor learning. While the sample size (n=4) was not large enough to determine any conclusive results, this paradigm may be useful in determining the neural mechanisms of bimanual learning and coordination in future studies. Similar to the unimanual mechanisms described above, motor learning of a bimanual coordination strategy requires dual activation of the brain hemispheres (Gooijers and Swinnen 2014; Swinnen 2002). Handedness is also thought to play an important role in these neural requirements with right-hand dominance relying more heavily on processes in the left hemisphere and left-hand dominance requiring greater hemisphere cooperation (Serrien et al. 2003). Prior studies have coupled electroencephalogram recordings with bimanual learning tasks and confirmed inseparable interhemispheric coupling involved (Andres et al. 1999; Manganotti et al. 1998). In their study of bimanual finger tapping, Andres et al. (1999) demonstrated a greater task-related hemispheric coherence (TRCoh; used as a measure of inter-regional functional coupling) in bimanual learning compared to unimanual learning. Interestingly, the bimanual TRCoh becomes more similar to unimanual levels as training progresses. Moreover, the data from this study suggests a cortical network involved in bimanual sequence learning: the bilateral SM1, SMA, CMA, PMd and PPC. Activation of these cortical areas has previously been demonstrated during complex unimanual and bimanual motor tasks (for review see Gerlof and Andres 2002). The electroencephalogram (EEG) mapping seen in Figure 13 further provides evidence for the

uniquely consequential involvement of the corpus callosum (for review see Gooijers and Swinnen 2014). While there is a wealth of information examining the neural substrates underlying bimanual learning, there is a substantial gap linking the neural activation patterns, the quantitative behavioral measures, and the computational models depicting the behavior.

6.2: Future Aims

The work set forth in this thesis will be expanded upon in future studies conducted at the Sensorimotor Integration Lab in collaboration with the Center for Mind and Brain and other facilities at the University of California, Davis with the aim of closing the gap outlined above. Plans for future investigation include analyzing adaptation of inter-manual coordination during manipulations of a single object perturbed using (1) visual feedback manipulations (outlined in Chapter 5) and (2) force perturbations (Figure 14). In addition, the lab aims (3) to concurrently measure electroencephalogram (EEG) signals during these two tasks in order to relate the behavior to brain activation patterns across tasks (visual vs. force) and limbs (dominant vs. non-dominant). The aim for experiments (1) and (2) are to examine how human subjects adapt

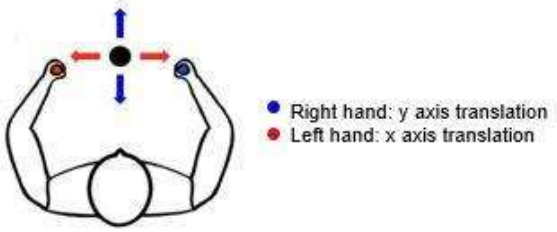

Figure 14: Joint bimanual coordination of object using force. The participant uses the right hand to control the cursor trajectory on the y axis and the left hand to control the trajectory over the x axis.

distributed control of an object in response to visual and force manipulations, respectively. We hypothesize that subjects will demonstrate an equal contribution by both hands during unperturbed trials, but when faced with the perturbation, an asymmetry in behavior and neural activation will occur with the non-dominant hand over-correcting for the disturbance. In task (2), we hypothesize gain dependent corrections made by both the perturbed and unperturbed hand

so as to minimize the single limb disturbance (Diedrichsen 2007). Utilizing EEG during these experiments (3) is hypothesized to yield different patterns of activation in each respective hemisphere dependent on the demands on the limb. For example, compared to simple arm reaching, coupled activity between PMC and M1 in the non-dominant hemisphere will correlate with task complexity (e.g., non-dominant limb control of object orientation and dominant limb control of trajectory). Aligned with previous studies, activity in the AIP is expected to be coupled with the PMC in response to the complex motor planning required (Stewart et al. 2013), and the PMC in combination with the left dorsolateral PFC being largely responsible for selection of action in both tasks.

The development of a computational framework to describe the distribution of control between the limbs could be applied to other complex behaviors. Additionally, the findings could further clinical studies aimed at understanding neurodegenerative disorders by helping to define behavioral biomarkers for early detection (e.g. Huntington's Disease). Furthermore, the potential findings could be applied to help understand the natural development of bimanual control, especially when one limb is impaired (e.g., pediatric upper limb deformities). Finally, this research has potential applications in robotics and assistive devices; a deeper understanding of how the two limbs work together, and the brain activity associated with this coordination, could aid brain machine interface efforts, and provide a foundation for human-robot interactions yet to be realized (e.g., utilizing an assistive robotic third limb).

References

Akaike H. A new look at the statistical model identification. IEEE TransAutomat Contr19: 716–723, 1974. Doi: 10.1109/TAC.1974.1100705

Anguera JA, Russell CA, Noll DC, Seidler RD. Neural correlates associated with intermanual transfer of sensorimotor adaptation. Brain Research 11845: 136-151. 2007. doi: 10.1016/j.brainres.2007.09.088

Arce F, Novick I, Mandelblat-Cerf Y, Israel Z, Ghez C, Vaadla E. Combined adaptiveness of specific motor cortical ensembles underlies learning. J Neurosci 30(15):5415-5425. 2010. doi:10.1523/JNEUROSCI.0076-10.2010

Andres FG, Mima T, Schulman AE, Duchgans J, Hallett M, Gerloff C. Functional coupling of human cortical sensorimotor areas during bimanual skill acquisition. Brain 122, 855–870 (1999).

Berniker M, Kording K. Estimating the sources of motor errors for adaptation and generalization. Nature Neuroscience 11: 1454-1461. 2008. doi:10.1038/nn.2229

Bindra G, Brower R, North R, Zhou W, Joiner WM. Normal Aging Affects the Short-Term Temporal Stability of Implicit, but not Explicit Motor Learning following Visuomotor Adaptation. eNeuro 2021. doi: 10.1523/ENEURO.0527-20.2021

Bond KM, Taylor JA. Flexible explicit but rigid implicit learning in a visuomotor adaptation task. J Neurophysiol 113(10):3836-49. doi:10.1152/jn.00009.2015.

Brayanov JB, Press DZ, Smith MA. Motor memory is encoded as a gain-field combination of intrinsic and extrinsic action representations. J Neurosci 32(43):14951-14965. 2012. doi:10.1523/JNEUROSCI.1928-12.2012

Carroll TJ, Poh E, de Rugy A. New visuomotor maps are immediately available to the opposite limb. J Neurophysiol 2014. Doi:10.1152/jn.00042.2014

Choe CS, Welch RB. Variables affecting the intermanual transfer and decay of prism adaptation. Journal of Experimental Psychology 102: 1076-1084. 1974.

Criscimagna-Hemminger SE, Donchin O, Gazzaniga MS, Shadmehr R. Learned dynamics of reaching movements generalize from dominant to nondominant arm. J Neurophysiol 89:168-176. 2003. doi:10.1152/jn.00622.2002

Day KA, Roemmich RT, Taylor JA, Bastian AJ. Visuomotor learning generalizes around the intended movement. ENeuro 3(2): 1-12. 2016. doi:10.1523/ENEURO.0005-16.2016

De Xivry JJO, Marko MK, Pekny SE, Pastor D, Izawa J, Celnik P, Shadmehr R. Stimulation of the Human Motor Cortex Alters Generalization Patterns of Motor Learning. J Neurosci 31(19):7102-7110. 2011. DOI:10.1523/JNEUROSCI.0273-11.2011

Donchin O, Gribova A, Steinberg O, Bergman H, de Oliveira CS, Vaadia E. Local field potentials related to bimanual movements in the primary and supplementary motor cortices. Exp Brain Res 140: 46-55. 2001. doi:10.1007/s002210100784

Diedrichsen J. Optimal Task-Dependent Changes of Bimanual Feedback Control and Adaptation. Current Biology 17(19):1675-1679. 2007. doi:10.1016/j.cub.2007.08.051

Eliassen JC, Baynes K, Gazzaniga MS. Anterior and posterior callosal contributions to simultaneous bimanual movements of the hands and fingers Brain, 123: 2501-2511. 2000. doi:10.1093/brain/123.12.2501

Gerloff C, Andres FG. Bimanual Coordination and Interhemispheric Interaction. Acta Psychologica 110: 161-186. 2002. doi:10.1016/S0001-6918(02)00032-X

Gonzales Castro LN, Monsen CB, Smith MA. The binding of learning to action in motor adaptation. PLoS Comput Biol 7(6): e1002052 doi:10.1371/journal.pcbi.1002052

Gooijers J, Swinnen SP. Interactions between brain structure and behavior: the corpus callosum and bimanual coordination. Neuroscience & Biobehavioral Reviews 43:1-19. 2014. doi:10.1016/j.neubiorev.2014.03.008

Hadjiosif AM, Smith MA. Generalization of the temporally-labile and temporally-stable components of motor memory (Abstract). Neuroscience Meeting Planner2013: 78.23, 2013.

Hwang EJ, Smith MA, Shadmehr R. Adaptation and generalization in acceleration-dependent force fields. Exp Brain Res 169: 496-506. 2006. doi:10.1007/s00221-005-0163-2

Joiner WM, Brayanov JB, Smith MA. The training schedule affects the stability, not the magnitude, of the inter-limb transfer of learned dynamics. J Neurophysiol 110(4):984-998. 2013. doi: 10.1152/jn.01072.2012

Kitago T, Ryan SL, Mazzoni P, Krakauer JW, Haith AM. Unlearning versus savings in visuomotor adaptation: comparing effects of washout, passage of time, and removal of errors on motor memory. Front Hum Neurosci. 2013 Jun 28;7:307. doi:10.3389/fnhum.2013.00307.

Krakauer JW, Pine ZM, Ghilardi MF, Ghez C. Learning of visuomotor transformations for vectorial planning of reaching trajectories. J Neurosci 20(23):8916-8924. 2000.

Manganotti P, Gerloff C, Toro C, Katsuta H, Sadato N, Zhuang P, Leocani L, Hallet M. Task-related coherence and task-related spectral power changes during sequential finger movements. Electroencephalography and Clinical Neurophysiology, 109: 50-62. 1998.

Malfait N, Ostry DJ. Is inter-limb transfer of force-field adaptation a cognitive response to the sudden introduction of load. J Neurosci 24(37):8084-8089. 2004. DOI:10.1523/JNEUROSCI.1742-04.200

McDougle SD, Bond KM, Taylor JA. Implications of plan-based generalization in sensorimotor adaptation. J Neurophysiol118: 383–393, 2017.doi:10.1152/jn.00974.2016

Morton SM, Lang CE, Bastian AJ. Inter- and intra-limb generalization of adaptation during catching. Exp Brain Res 141:438-445. 2001. DOI: 10.1007/s002210100889

Norris SA, Greger BE, Martin TA, Thach WT. Prism adaptation of reaching is dependent on the type of visual feedback of hand and target position. Brain Research 905:207-219. 2001. doi: S0006-8993(01)02552-5

Nozaki D, Kurtzer I, Scott S. Limited transfer of learning between unimanual and bimanual skills within the same limb. Nat Neurosci 9, 1364–1366 (2006). https://doi.org/10.1038/nn1785

Paz R, Nathan C, Boraud T, Bergman H, Vaadia E. Acquisition and generalization of visuomotor transformations by nonhuman primates. Exp Brain Res 161:209-219. 2005. doi:10.1007/s00221-004-2061-4

Poh E, Carroll TJ, Taylor JA. Effect of coordinate frame compatibility on the transfer of implicit and explicit learning across limbs. J Neurophysiol 116:1239-1249. 2016. doi:10.1152/jn.00410.2016.

Rezazadeh A, Berniker M. Force-field generalization and the internal representation of motor learning. Plos One. 2019. doi:10.1371/journal.pone.0225002

Sainburg RL, Wang J. Inter-limb transfer of visuomotor rotations: independence of direction and final position information. Exp Brain Res 145: 437-447. 2002. doi: 10.1007/s00221-002-1140-7

Schulze K, Luders E. Jancke L. Intermanual transfer in a simple motor task. Cortex 38:805-815. 2002.

Serrien DJ, Sovijarvi-Spape MM, Farnsworth B. Bimanual control processes and the role of handedness. Neuropsych 26(6)802-7. 2012. doi: 10.1037/a0030154.

Shadmehr R. Generalization as a behavioral window to the neural mechanisms of learning internal models. J Hum Mov Sci 23:543-568. 2004. doi:10.1016/j.humov.2004.04.003

Shadmehr R, Moussa-Ivaldi FA. Adaptive Representation of Dynamics during Learning of a Motor Task. J Neurosci 14(5):3208-3224. 1994.

Shadmehr R, Moussavi ZMK. Spatial Generalization from Learning Dynamics of Reaching Movements. J Neurosci 20(20):7807-7815. 2000.

Shadmehr R, Smith MA, Krakauer JW. Error Correction, Sensory Prediction, and Adaptation in Motor Control. Annual Review of Neuroscience 22:89-108. 2010. doi: 10.1146/annurev-neuro-060909-153135

Stewart BM, Baugh LA, Gallivan JP, Flanagan JR. Simultaneous encoding of the direction and orientation of potential targets during reach planning: evidence of multiple competing reach plans. J Neurophysiol 110(4):807-816. 2013. doi:10.1152/jn.00131.2013

Swinnen SP. Intermanual coordination: from behavioural principles to neural-network interactions. Nature Reviews. 3:350-361. 2002.

Swinnen SP, Wenderoth N. Two hands, one brain: cognitive neuroscience of bimanual skill. Trends in Cognitive Sciences 8:18-25. 2004. doi:10.1016/j.tics.2003.10.017

Tanaka H, Sejnowski TJ, Krakauer JW. Adaptation to Visuomotor Rotation Through Interaction Between Posterior Parietal and Motor Cortical Areas. J Neurophysiol 102(5):2921-2932. 2009. doi:10.1152/jn.90834.2008

Taylor JA, Hieber LL, Ivry R.B. Feedback-dependent generalization. J Neurophysiol 109: 202-215. 2013. doi:10.1152/jn.00247.2012

Taylor JA, Krakauer JW, Ivry RB. Explicit and implicit contributions to learning in a sensorimotor adaptation task. J Neurosci 34(8):3023-3032. 2014. DOI:10.1523/JNEUROSCI.3619-13.2014

Taylor JA, Wojaczynski GJ, Ivry RB. Trial-by-trial analysis of intermanual transfer during visuomotor adaptation. J Neurophysiol 106: 3157–3172, 2011.

Wang J, Joshi M, Lei Y. The extent of inter-limb transfer following adaptation to a novel visuomotor condition does not depend on awareness of the condition. J Neurophysiol 106: 259–264, 2011.

Wang J, Sainburg RL. Limitations in inter-limb transfer of visuomotor rotations. Exp Brain Res 155:1-8. 2004. DOI 10.1007/s00221-003-1691-2

Wise SP, Moody SJ, Blomstrom KJ, Mitz AR. Changes in motor cortical activity during visuomotor adaptation. Exp Brain Res 121: 285-299. 1998.

Zhou W, Fitzgerald J, Colucci-Chang K, Murthy KG, Joiner WM. The temporal stability of visuomotor adaptation generalization. J Neurophysiol 118: 2435-2447. 2017. doi: 10.1152/jn.00822.2016